# Neural Dynamics in a Model of the Thalamocortical System. I. Layers, Loops and the Emergence of Fast Synchronous Rhythms

Erik D. Lumer, Gerald M. Edelman and Giulio Tononi

The Neurosciences Institute, 10640 John Jay Hopkins Drive, San Diego, CA 92121, USA

A large-scale computer model was constructed to gain insight into the structural basis for the generation of fast synchronous rhythms (20–60 Hz) in the thalamocortical system. The model consisted of 65 000 spiking neurons organized topographically to represent sectors of a primary and secondary area of mammalian visual cortex, and two associated regions of the dorsal thalamus and the thalamic reticular nucleus. Cortical neurons, both excitatory and inhibitory, were organized in supragranular layers, infragranular layers and layer IV. Reciprocal intra- and interlaminar, interareal, thalamocortical, corticothalamic and thalamoreticular connections were set up based on known anatomical constraints. Simulations of neuronal responses to visual input revealed sporadic epochs of synchronous oscillations involving all levels of the model, similar to the fast rhythms recorded *in vivo*. By systematically modifying physiological and structural parameters in the model, specific network properties were found to play a major role in the generation of this rhythmic activity. For example, fast synchronous rhythms could be sustained autonomously by lateral and interlaminar interactions within and among local cortical circuits. In addition, these oscillations were propagated to the thalamus and amplified by corticothalamocortical loops, including the thalamic reticular complex. Finally, synchronous oscillations were differentially affected by lesioning forward and backward interareal connections.

## Introduction

The thalamocortical system exhibits certain striking structural features that are remarkably constant across its various subdivisions and across different mammalian species. These include the organization of the cortex in multiple layers, and the presence of a complex system of reciprocal intra- and interlaminar, interareal, corticothalamic and thalamoreticular connections. Recent experimental evidence indicates that these structural features are associated with complex neuronal firing patterns produced during spontaneous activity (Steriade *et al.*, 1996a,b) and in relation to specific sensory (Gray and Singer, 1989; Singer, 1993; Sillito *et al.*, 1994) or sensory-motor tasks (Murthy and Fetz, 1992; Bressler *et al.*, 1993; Nicolelis *et al.*, 1995). In particular, rhythmic synchronous activity in the high-frequency range, involving widespread populations of neurons distributed through multiple thalamic and cortical levels, have been observed in the thalamocortical system of several mammalian species by recording electrocorticograms, evoked potentials, local field potentials and multiunit activity (Llinás and Ribary, 1993; Sillito *et al.*, 1994; Bressler, 1995; Neuenschwander and Singer, 1996; Steriade *et al.*, 1996b). It has been suggested that such synchronous activity plays a fundamental role in the functional integration of neural events occurring at multiple cortical sites (Milner, 1974; von der Malsburg, 1981; Damasio, 1989; Tononi *et al.*, 1992; Singer, 1993). However, the precise relationship between the anatomical and physiological properties of thalamocortical systems and their overall dynamics is not at all clear. The major

problem is the large number of parameters involved. It is, for example, extremely difficult to obtain an adequate understanding of the many interactions occurring at several levels in such systems. Modeling studies have therefore been employed to shed some light on specific functional questions (Bush and Douglas, 1991; Douglas *et al.*, 1991; Sporns *et al.*, 1991; Wörgötter and Koch, 1991; Tononi *et al.*, 1992; Wilson and Bower, 1992; Olshausen *et al.*, 1993; Destexhe *et al.*, 1994; Golomb *et al.*, 1994; Niebur and Koch, 1994; Douglas *et al.*, 1995; Nowlan and Sejnowski, 1995; Somers *et al.*, 1995). However, no detailed extant model emphasizes the overall structural organization of thalamocortical systems in conjunction with realistic cellular and synaptic properties. To overcome this barrier, we introduce a large-scale model that provides the minimum features that seem necessary for operation of the basic thalamocortical circuitry (Diamond and Hall, 1969; Zeki and Shipp, 1988). These include distinct populations of excitatory and inhibitory cells, grouped in layers in the cortex and in the thalamus, and various sets of intra- and interareal reciprocal connections with layer-specific patterns of origin and termination. Among these, certain prominent 'vertical loops' and 'horizontal networks' stand out as key components of the thalamocortical circuitry: loops between cortical areas and their associated thalamic nuclei that incorporate the reticular thalamic complex; intracortical loops that link infragranular and supragranular layers; networks of inhibitory interneurons and patchy networks of long-range excitatory connections that spread horizontally within each cortical area; and extensive reciprocal connectivity between cortical areas.

The form of this model is sufficiently general that it can apply, with suitable adjustments, to most thalamocortical subdivisions, and as such has the properties of a prototypical thalamocortical system. At the same time, it specifically incorporates properties of the much studied cat visual system in sufficient detail to allow a direct comparison with the results of intra- and extracellular recordings. It therefore can be used to explore the relationships between anatomical and physiological aspects of the thalamocortical system and its neural dynamics. In particular, this model provides a unique opportunity to investigate the specific role of different cortical layers and of cortical and corticothalamic loops in generating synchronous rhythms.

We first describe the anatomical and physiological constraints incorporated in the model, and then go on to show that fast synchronous oscillations emerge naturally from these constraints, even though the model was not designed to produce specific dynamics. By simultaneously observing the activity of thousands of simulated neurons, we find that these rhythms span different cortical layers, different cortical areas, and arise between the cortex and thalamic regions, in a fashion similar to the fast rhythms recorded *in vivo*. We then make use of the model to investigate the mechanisms involved in the generation

of these coherent firing patterns. The results suggest that, while both the intrinsic membrane properties of neurons and the local interplay of excitation and inhibition may be involved in the generation of synchronous rhythmic activity, several additional components of the thalamocortical circuitry, namely the long-range horizontal cortical networks, and the interlaminar, corticocortical and thalamocortical loops, interact in a complex manner to promote and sustain fast synchronous activity. These results form the basis for an investigation, in a companion paper, of the functional significance of synchronous activity distributed through multiple levels of a sensory pathway.

## Materials and Methods

### Overview of the Model

Figure 1 shows the overall architecture of the model. The model had ~65 000 spiking neurons with ~5 million connections organized in regions and pathways respectively. The modeled regions consisted of in-register sectors in a primary and a secondary area of visual cortex (Vp and Vs), two corresponding regions of the dorsal thalamus (Tp and Ts), and two regions of the reticular thalamic nucleus (Rp and Rs). Vp represented a restricted portion of area 17 in the cat (i.e. ~1 cm$^2$) and contained units with small receptive fields that were selective for oriented segments. Vs represented a corresponding part of an extrastriate area with coarser topography, containing units with larger receptive fields that were selective for oriented lines and for line crossings. Tp and Ts corresponded respectively to a portion of the lateral geniculate nucleus (LGN) and to a portion of the lateral posterior pulvinar complex (LP). A reticular nucleus (RT) was intercalated between the cortex and the thalamus.

A central feature of the model is the subdivision of the simulated cortex into three laminae with different patterns of afferent, efferent and local connectivity (Fig. 1). These laminae corresponded to supragranular layers, infragranular layers, and layer IV respectively. Another important feature of the model is the emphasis on the detailed simulation of various sets of connections that link cortical and thalamic areas, as well as of connections intrinsic to these regions. The model included horizontal intralaminar connections, vertical interlaminar connections within Vp and Vs, forward and backward connections between Vp and Vs, thalamocortical and corticothalamic connections, and connections from thalamic relay nuclei and cortex to the nucleus reticularis. Individual neurons, both excitatory and inhibitory, were modeled as single-compartment integrate-and-fire units using cellular constants from regular-spiking and fast-spiking neurons respectively (Connors *et al.*, 1982). Synaptic interactions occurred through simulated channels that provided voltage-dependent (NMDA-like) and voltage-independent (AMPA-like) excitation, as well as fast (GABA$_A$-like) and slow (GABA$_B$-like) inhibition. All connections were endowed with conduction delays.

In the following sections, we describe the principles used to construct and scale the simulated cortical and thalamic regions, the layout of the various connection pathways within and among these regions, and the implementation of cellular and synaptic properties. We then describe the stimuli used to activate the model, the procedures for the collection and analysis of data, and the actual computer implementation.

### Regional Organization

#### Primary Cortical Area

Vp represented a portion of visual area 17. In the cat, for example, the striate cortex exhibits a basic periodicity of structure and function at the scale of ~1 mm. This organization is manifested both in terms of the center-to-center distance of iso-orientation bands, which averages 1.1 mm in the cat (Löwel *et al.*, 1987; Kisvárday and Eysel, 1993) and in terms of the average separation of neighboring axonal patches in supragranular layers (Kisvárday and Eysel, 1992). To constrain our model, we assumed that an area of ~1.1 mm$^2$ forms a basic macro-unit in the striate cortical mosaic array. Vp was scaled to span 64 (8 × 8) such macro-units. We assumed that each macro-unit can be divided in discrete groups of neurons corresponding to 32 different combinations of response selectivities, at each topographic location. These response selectivities
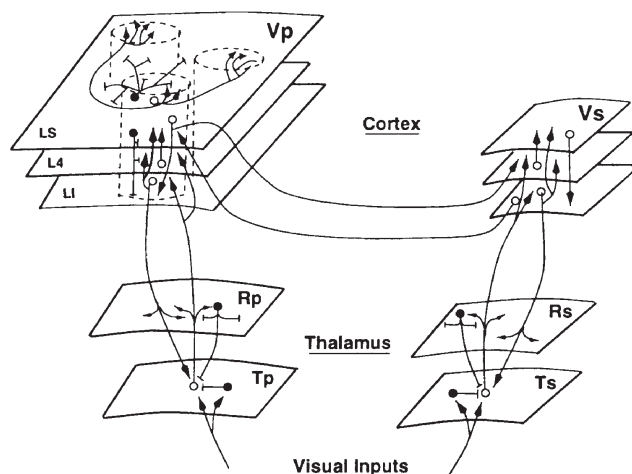


**Figure 1.** Schematic diagram of the various types of connections involved in the thalamocortical model. Excitatory and inhibitory cells are depicted with the use of open and filled circles respectively. (i) Thalamocortical loops: thalamocortical pathways ascend in parallel from Tp to Vp and Ts to Vs, with terminations in the infragranular layer (LI) and layer IV (L4). En passant contacts from Tp and Ts are made in Rp and Rs. Thalamocortical pathways are reciprocated by corticothalamic projections originating in LI. En route, such fibers give collaterals to their associated RT sector. (ii) RT networks: RT cells are embedded in a diffuse inhibitory synaptic network. Projections from RT to thalamocortical neurons are also diffuse. (iii) Intracortical loops: columnar projections are made from L4 to the supragranular layer (LS), from LS to LI, and from LI back to L4 and LS. (iv) Networks of long-range horizontal connections within each cortical layer. Unlike inhibitory contacts, these excitatory projections are restricted to patches of cells with similar selectivities. (v) Interareal corticocortical loops: forward projections ascend from LS of Vp to L4 of Vs; backward projections descend from LI of Vs to LS of Vp.

correspond to all possible combinations of two inputs, from left or right eye, two pathways, e.g. the X- and Y-thalamocortical pathways, and eight subdivisions of the range of orientations. In the present study, we modeled two of these 32 response selectivities, namely the vertical and horizontal orientation for the X pathway of one eye. In addition, Vp was visuotopically organized at a finer spatial scale. We assumed that, for each selectivity within a macro-unit, there was a collection of 5 × 5 topographic elements, each of which corresponded to a contiguous location in retinal space. Each collection of 5 × 5 elements thus corresponded to the central part of a patch of visual cortex in which nearby neurons have similar orientation selectivity and continuously varying receptive field locations. Topographic elements in Vp were organized in maps of 40 × 40 elements for each of the two modeled orientation selectivities. Each topographic element contained 10 neurons organized in three laminae — supragranular, infragranular and layer IV. The infragranular layer and layer IV in each element contained two excitatory cells and one inhibitory cell, while the supragranular layer contained two excitatory cells and two inhibitory cells with different connectivities. Note that while the ratio between modeled excitatory and inhibitory neurons was comparatively low due to computer limitations, a more important parameter at the network level is the ratio between excitatory and inhibitory synapses, which in the model was close to the values observed in the brain (see below). The subdivision of the modeled cortical areas in elements spanning all layers reflects the developmental, anatomical and physiological evidence for a basic columnar organization of neocortex (Mountcastle, 1957; Gilbert, 1993; Rakic, 1995).

Overall, Vp corresponded to ~0.8 cm$^2$ of striate cortical surface and spanned a monocular patch of 8° × 8° in the parafoveal visual field. Each topographic element in the model would thus correspond to a cortical column containing a total of ~94 neurons with a surface area of 1454 μm$^2$. This was calculated assuming that different selectivities are mapped onto non-overlapping pieces of cortex, and that there are ~62 000 neurons beneath 1 mm$^2$ of cortical surface in area 17 (Beaulieu and Colonnier,

1983). Since for each topographic element we explicitly simulated 10 cells, each such cell represented the activity of nine cortical neurons. On the basis of the clustering of apical dendrites of layer V and layer II/III pyramidal cells, Peters and Yilmaz (1993) have proposed that the basic anatomical unit in the cortex is a module containing, in the case of the cat, some 200 neurons that are grouped beneath 2500 $\mu m^2$ of cortical surface. Thus, the topographic elements in the model are comparable to these basic cortical modules.

### Secondary Cortical Area

The secondary visual area (Vs) was taken to correspond to an extrastriate area located along the ventral occipitotemporal pathway. Although Vs did not represent in detail any particular region of visual cortex, we used, as a reference, area 21 in the cat, which is the presumed homolog of cortical area V4 in the monkey (Payne, 1993). Vs was assumed to be about half the size of Vp [in the monkey, V1 is 1120 $mm^2$ and V4 is 540 $mm^2$ (Felleman and Van Essen, 1991)]. In the model, Vs was constructed based on some general properties associated with extrastriate areas (e.g. an enlargement of receptive fields) and with termination patterns of 'forward' and 'backward' corticocortical projections (Felleman and Van Essen, 1991). Vs contained neurons that were selective for either vertical lines, horizontal lines or line crossings, organized in a coarse topographic map. For each of its three selectivities, Vs had a map of 30 × 30 elements as compared to the 40 × 40 elements in Vp.

### Thalamic Sectors

According to Peters and Payne (1993), there is a rough correspondence between the number of X-cells in the LGN and the number of basic cortical modules in area 17. We therefore modeled a geniculate map (Tp) comprised of the same number of elements (40 × 40) as each of the two maps in Vp. Each element of Tp contained two modeled neurons which correspond respectively to an X-relay cell and to an inhibitory interneuron. For simplicity of implementation, only the ON-portion of thalamic receptive fields was modeled. The secondary thalamic map (Ts) had 30 × 30 elements and its visuotopic arrangement had a much lower spatial resolution than in Tp. Two reticular thalamic sectors, Rp and Rs, were modeled respectively as a 40 × 40 and a 30 × 30 map of inhibitory neurons.

### Connectivity

In constructing the model, special emphasis was put on the incorporation of realistic network properties, such as the spread and relative proportions of the various sets of connections composing the intra- and interregional thalamocortical circuitry. Specific patterns of arborization were classified as either focused or diffuse, on the basis of anatomical data. The focused connection pattern diverged for single arbors over a topographically registered region of 5 × 5 target elements. Diffuse projections typically covered an area of 25 × 25 elements for a single arbor. Contacts from individual arbors in the target area were made probabilistically according to spatial density profiles with exponential fall-off. The proportion of synapses from different sources was used as a constraint in the parameterization of the various density profiles. This parameterization is detailed in the Appendix.

### Horizontal Intralaminar Connections

Individual excitatory neurons in the supragranular layers of striate cortex have intralaminar horizontal projections that tend to be organized in patches of 200–400 $\mu m$ in diameter. These patches typically interconnect neurons that have similar orientation preference (Kisvárday and Eysel, 1992). Patches originating from a single location extend over a region of ~2–4 mm (Gilbert, 1993). In the model, horizontal connections in the supragranular layer of Vp were made diffusely onto iso-orientation cells, with an equivalent spread of 5.5 × 5.5 $mm^2$. Intrinsic connections in the infragranular layer of Vp had a similar organization. Intralaminar connections in layer IV extended over a more limited area of 15 × 15 elements. This reduced projective field reflected the more compact arborization in layer IV (Douglas and Martin, 1990).

### Vertical Interlaminar Connections

Interlaminar connections couple neurons vertically through the cortical depth. These connections may be described as part of a loop that includes the following major steps (Gilbert, 1993): from layer IV to supragranular layers, from supragranular to infragranular layers, and from infragranular back to layer IV and to supragranular layers (Callaway and Wiser, 1994; Wiser and Callaway, 1994). All these projections were made in a focused manner in the model. As a further constraint, we considered the proportion of synapses from different sources in each layer. As an example, for each simulated excitatory cell of layer IV, there were on the average 40 interlaminar connections from infragranular layer and 23 intralaminar connections from layer IV, in close agreement with the 45%/28% ratio reported in the cat striate cortex (Ahmed et al., 1994). A similar connectivity was established in each map of Vs.

### Intracortical Inhibitory Connections

The cerebral cortex comprises many different types of GABAergic inhibitory interneurons (Douglas and Martin, 1990; Jones, 1993). Among these, basket cells are ubiquitous and project mostly to the same layer where their soma is located. Double-bouquet cells are concentrated in supragranular layers (Condé et al., 1994; Kawaguchi, 1995) and their projections are organized in a restricted columnar arrangement which extends to most layers. There are indications that basket cells and other inhibitory interneurons act through fast $GABA_A$ receptors, while double-bouquet cells may preferentially activate $GABA_B$ receptors (Kang et al., 1994). In the model, basket-like cells provided a fast ($GABA_A$-like) inhibition within each cortical layer to all cell types; double-bouquet analogs located in supragranular layers provided a slow ($GABA_B$-like) inhibitory control of a narrow cylinder extended to all three laminae.

The relationship between inhibition and orientation selectivity in the visual cortex is complicated. However, some recent studies suggest that a single basket cell in the cat visual cortex provides input to surrounding regions representing the whole range of orientations, including iso- and cross-orientations to that basket cell soma (Kisvárday and Eysel, 1993; Kisvárday et al., 1994). In the model, we assumed that lateral inhibition ($GABA_A$) was provided equally to both of the modeled orientation selectivities in Vp. In Vs, half of the terminals of individual basket-like cells in Vs provided input to cells with similar selectivity to that of the parent soma, while the remaining half were split evenly between cells of other selectivities. The density profile of inhibitory connections was adjusted such that the relative proportions of inhibitory connections per layer was around the values reported in the literature, i.e. ~10–20% of all synapses (Beaulieu and Colonnier, 1985; Beaulieu et al., 1992).

### Forward and Backward Interareal Connections

According to several studies, backward connections are considerably more divergent than forward connections. This has been documented for projections from area MT to V1 and V2 of primates (Krubitzer and Kaas, 1989; Shipp and Zeki, 1989; Zeki and Shipp, 1989), and from V2 to V1 (Rockland and Virga, 1989; Henry et al., 1990; Rockland and Hoesen, 1994). Reconstructions of single axons indicate that forward projections from V1 and V2 to V4 have discrete terminal clusters (2–4 clusters per axon, 250 $\mu m$ wide), which are distributed over 2–2.5 mm (Rockland and Virga, 1989; Rockland, 1992). Conversely, individual axons from V4 to V1 diverge up to 5 mm (Rockland et al., 1994). These values should be compared to values of ~2–5 mm for horizontal connections in V1. According to a classic description, forward projections tend to originate in superficial layers and to terminate in layer IV, while backward connections tend to originate from infragranular as well as supragranular layers and to terminate outside layer IV (Rockland and Pandya, 1979). This basic scheme has since become considerably more complicated (Maunsell and Van Essen, 1983; Felleman and Van Essen, 1991). In the model, forward connections originating from the supragranular layer of Vp defined the three feature-specific responses in Vs. These selectivities resulted from biased convergent projections onto individual layer IV neurons of Vs from either a 19 × 3 region of vertical selective cells, a 3 × 19 region of horizontal selective cells, or from both selectivities of Vp (9 × 3 and 3 × 9 regions respectively). Backward projections from vertical and horizontal selective cells of Vs originated in the infragranular layer and terminated diffusely in the supragranular layer of Vp, targeting cells of similar orientation specificity. In contrast, backward projections from cross-selective cells extended to both selectivities in Vp. The laminar

specificity of projections between Vp and Vs was consistent with that observed between cat areas 17 and 21 (Rosenquist, 1985).

### Thalamic Connections

Relay cells project directly out of their thalamic nuclei, while local interneurons in these structures inhibit other interneurons as well as relay cells with a focused connectivity pattern. RT neurons make diffuse connections within the RT nucleus and in thalamic relay nuclei (Dubin and Cleland, 1977). The axons of thalamic relay cells send out collaterals to the reticular nucleus. In the model, local interneurons produced (fast) $GABA_A$-mediated IPSPs in thalamocortical relay cells. Thalamic to reticular projections, i.e. from Tp to Rp and from Ts to Rs, were made according to the focused connection scheme. RT projections targeted their corresponding relay sectors of the thalamus in a diffuse manner. The RT inhibition of relay neurons was mediated by $GABA_A$ IPSPs, in agreement with the dominant form of inhibition observed when RT cells fire tonically (Pinault and Deschênes, 1992).

### Thalamocortical and Corticothalamic Connections

X-cells in cat laminae A and A1 of the LGN send axons that terminate mainly in layer IV and VI of area 17 (LeVay and Gilbert, 1976; Leventhal, 1979; Freund et al., 1985). In the model, each simulated cell in layer IV of Vp received connections spread over a 8 × 2 region of the thalamic map for the vertical selectivity (2 × 8 for the horizontal selectivity). Infragranular cells received about half as many connections from the same geniculate regions. The anisotropic arrangement of these projections promoted orientation-specific cortical responses. Note that, in the model, the same X axon targeted both horizontal and vertical cortical cells, such that its arbor extended over at least half of an orientation cycle or 0.55 mm. This dimension is consistent with anatomical evidence that X axonal terminals form a single elongated clump in area 17, ~1 mm long × 0.6–0.8 mm wide (Freund et al., 1985). Vs cells in layer IV and the infragranular layer received thalamocortical projections converging from a 4 × 4 region of Ts. Thalamocortical projections accounted for ~8% of all connections received by layer IV neurons, consistent with anatomical estimates (Peters and Payne, 1993; Ahmed et al., 1994). Corticothalamic axons descended from the infragranular excitatory cells into their corresponding thalamic relay sectors, contacting all cell types present in these structures, consistent with anatomical data (Robson, 1983; Weber et al., 1989; Montero, 1991). En route, such fibers sent collaterals to the RT nucleus. The topography of corticothalamic connectivity matched that of the thalamocortical connectivity (e.g. see Jones, 1985).

### Cellular and Synaptic Physiology

#### Neurons

Individual neurons, both excitatory and inhibitory, were modeled as single-compartment integrate-and-fire units using cellular constants from regular- and fast-spiking neurons respectively (Connors et al., 1982). The instantaneous change of the membrane potential of each model neuron $i$, $V_i(t)$, was given by

$$\tau_m dV_i(t)/dt = -V_i + E_0 - \sum_j g_j(t)\left(V_i - E_j\right)$$

where $\tau_m$ is a passive membrane time constant set at 16 ms (8 ms respectively) for cortical excitatory (inhibitory) cells, and the sum on the right-hand side is of synaptic currents. These membrane time constants were consistent with experimental data (Connors et al., 1982; Mason et al., 1991; Baranyi et al., 1993; Kim and Connors, 1993). $E_0$ denotes the passive resting potential which was set to a value of –60 mV in agreement with in vivo measurements (Douglas et al., 1991; Ferster and Jagadeesh, 1992). $V_i$ was reset to the potassium reversal potential, $E_K$ = –90 mV, when it exceeded a threshold of either –51 mV (excitatory units) or –52 mV (inhibitory units), at which point a spike was recorded, and relayed with a transmission delay to appropriate synaptic targets.

#### Synapses

Simulated synaptic channels provided voltage-dependent (NMDA-like)

and voltage independent (AMPA-like) excitation, as well as fast ($GABA_A$-like) and slow ($GABA_B$-like) inhibition. Synaptic activation was expressed as a change of a channel conductance, $g(t)$, according to a dual exponential response to single spike events given by:

$$g(t) = g_{peak} \frac{e^{-t/\tau_1} - e^{-t/\tau_2}}{e^{-t_{peak}/\tau_1} - e^{-t_{peak}/\tau_2}}$$

with $\tau_1$ and $\tau_2$, the rise and decay time constants respectively, and $t_{peak}$ the time to peak:

$$t_{peak} = \frac{\tau_1 \tau_2}{\tau_1 - \tau_2}$$

Conductances were implicitly normalized by a leak membrane conductance, so that they were adimensional. The time constants and reversal potential ($E_j$) for each channel type were taken from the neurophysiological literature (Otis and Mody, 1992; Stern et al., 1992; Otis et al., 1993). The peak conductances, $g_{peak}$, were chosen to conform to a few simple constraints which led to regular network behavior. These constraints consisted of having: (i) peak EPSPs of 1 mV in AMPA-like channels; (ii) matched integrated EPSCs through AMPA and unblocked NMDA channels; (iii) matched integrated IPSCs through $GABA_A$ and $GABA_B$ channels. The activation of NMDA-like channels was expressed as:

$$\tilde{g}_{NDMA}(t) = m(V)g_{NDMA}(t)$$

where $g_{NMDA}(t)$ is a dual exponential impulse response and $m(V)$ is a sigmoidal function of the postsynaptic membrane potential. The modulation term was zero at membrane potentials lower than –53 mV and was maximal above the excitatory firing threshold. This modulation reflects the voltage-dependent affinity of the $Mg^{2+}$ located inside the channel pore. Specific parameter settings for the different type of synaptic channels are listed in Table 1.

AMPA-like channels were used for most excitatory connections implemented in the model. For horizontal connections in supragranular layers, as well as for backward connections from Vs to supragranular cells of Vp, we used voltage-dependent NMDA-like channels. This choice enabled these connections to modulate the firing of target units without disrupting their response selectivity. Evidence supporting this choice includes the finding that voltage-gated NMDA receptors are denser in the supragranular layers of visual cortex (Fox et al., 1989; Rosier et al., 1993); in addition, the effectiveness of these connections seems in part contingent upon a concomitant depolarization of target cells that are not in visuotopic register with the sources of afferentation (Bullier et al., 1988; Hirsh and Gilbert, 1991; Salin and Bullier, 1995). Preliminary testing of the model indicated that this choice was not critical for the results reported here. Inhibition in the thalamus was mediated by fast ($GABA_A$-like) synapses. In the cortex, fast and slow inhibition originated from different cell types as described above.

#### Spontaneous Activity

In awake animals, spontaneous activity levels have been estimated at ~4 Hz for excitatory and ~15 Hz for inhibitory cells (Hertz et al., 1964; Sanseverino et al., 1973; Legéndy and Salcman, 1985; Swadlow, 1988; Eggermont, 1990; Oram and Perett, 1992). In the model, similar values of spontaneous activity were achieved by a Poissonian activation of synaptic channels, which also resulted in an average balance of synaptic excitation

**Table 1**

Synaptic channel parameters

| Receptor | $g_{peak}$ | $\tau_1$ (ms) | $\tau_2$ (ms) | $E$ (mV) |
|---|---|---|---|---|
| AMPA | 0.05 | 0.5 | 2.4 | 0 |
| $GABA_A$ | 0.175 | 1 | 7 | –70 |
| $GABA_B$ | 0.0017 | 30–90 | 170–230 | –90 |
| NMDA | 0.0075 | 4 | 40 | 0 |

**Table 2**
Synaptic noise

| Receptor | $\lambda_{spont}$ | $A_{spont}$ |
|----------|-------------------|-------------|
| AMPA | 0.425 | 4 |
| GABA$_A$ | 1.6 | 0.5 |
| GABA$_B$ | 0.645 | 0.125 |

$\lambda_{spont}$, event rate; $A_{spont}$, event amplitude.

and inhibition of individual cells. The parameters used to produce this spontaneous firing are summarized in Table 2. In addition, we modeled spike-frequency adaptation in cortical excitatory cells by activating a hyperpolarizing GABA$_B$-like channel each time a spike was emitted. With the above parameters, cortical excitatory and inhibitory units exhibited a behavior consistent with the recordings from regular and fast spiking neurons (Connors and Gutnick, 1990) respectively. For simplicity, all thalamic cells were modeled using the parameters of cortical inhibitory units. This choice led to firing characteristics similar to those of X-type geniculate cells (Kaplan *et al.*, 1987).

### Transmission Delays

When characterizing the transmission time of sensory signals between successive processing stages in the cortex, it is important to distinguish two components of the response in a given site elicited by the activation of another site. The earliest response component, which occurs in a few milliseconds, is typically associated with monosynaptic interactions. Its latency reflects the cumulative effects of axonal conduction delays, synaptic delays and the time necessary for the postsynaptic potential to reach threshold. After the initial response component, different types of lateral and interlaminar interactions of excitation and inhibition come into play. The time required for these polysynaptic processes to take effect is variable, depending on the type of stimulation and on the actual pathways involved. This late response component determines how soon a target area will be able to transmit the result of its afferent activation to other areas. Measured latencies between the firing of successive visual cortical areas in the cat have been estimated to lie between 5 and 15 ms (Dinse and Krüger, 1994) in the forward direction. Geniculocortical latencies may be even shorter (Bullier and Henry, 1979). Backward connections may be slower conducting. For instance, latencies from area 18 and 19 to area 17 were 6 and 10 ms respectively (Bullier *et al.*, 1988).

Given that in the model the simulated cortices contained only three layers (instead of six), we chose to account for these measured latencies along polysynaptic pathways by assuming comparatively longer transmission delays along certain pathways. Transmission delays for individual connections were sampled from Gaussian distributions with a standard deviation of 1 ms. Each set of connections in the model was associated with a specific mean delay. We assumed that the latency incurred by one synaptic step within a cortical area was on the order of 5 ms. Of this latency, 2 ms were attributed to the axonal and synaptic delays proper. Mean conduction delays were thus set to 2 ms for intralaminar connections and for most interlaminar connections. However, infragranular to layer IV connections were delayed on average by 7 ms, to account for disynaptic transmission through layers V and VI. Thalamocortical connections and forward connections from Vp to Vs had a mean delay of 3 ms, while corticothalamic connections and backward connections from Vs to Vp had a mean delay of 8 ms, again taking into account a disynaptic pathway through layers 5 and 6. The influence of assuming comparatively longer or shorter transmission delays from LI to L4, from Vs to Vp, and from cortex to thalamus is specifically tested in the Results.

### Stimuli

In a typical experiment, the model was presented with a simulated stimulus consisting of two superimposed gratings, one vertical and one horizontal, moving in perpendicular directions at 2 cycles/s. Stimulation was achieved by applying a stochastic (Poisson) synaptic excitation independently to each cell of Tp and Ts, that was rate-modulated according to the spatial structure of the gratings. In Tp, non-zero

activation with an amplitude equivalent to 10 synchronous EPSPs per synaptic event ($\lambda = 0.3$ kHz) was confined to bars of the gratings, which were two elements wide and spaced by eight elements in each grating. A corresponding pattern, suitably scaled down and blurred via a $5 \times 5$ Gaussian mask, was also used to stimulate Ts.

### Data Collection and Analysis

In a typical run, the model was presented for epochs of up to 2 s with a visual stimulus of the kind described above. The membrane potential, $V$, for all units in the model was recorded, and a number of population-averaged variables were computed. In particular, the average membrane potential, $V_{pop}$, was computed for chosen subsets of $N$ units in the model as:

$$V_{pop}(t) = \frac{1}{N}\sum_i V_i(t)$$

This variable, which is reminiscent of local field potentials (LFPs), has been used in a number of recent modeling studies as a useful indicator of synchronous activity (Destexhe *et al.*, 1994; Golomb *et al.*, 1994). To make population-averaged voltages and LFPs more readily comparable, spikes were removed from individual voltages by rectifying the membrane potentials at a threshold of –40 mV. Autocorrelograms of population-averaged membrane potentials were computed to assess the presence and main frequency of synchronous oscillations. Oscillatory frequencies were further characterized using power spectral estimates. Cross-correlograms of population-averaged potentials from non-overlapping neuronal populations were used to characterize phase relationships in their patterns of activation. These correlograms were calculated according to the formula:

$$CC_{12}(\tau) = \frac{1}{T}\int_{t_0}^{t_0+T}\left(V_{pop1}(t) - \langle V_{pop1}\rangle\right)\left(V_{pop2}(t+\tau) - \langle V_{pop2}\rangle\right)\mathrm{d}t$$

where $<V>$ designates a population- and time-averaged membrane potential. The autocorrelogram corresponds to the case where the populations pop1 and pop2 are identical.

### Computer Implementation

All simulations were performed with the use of CellLab, a general-purpose object-oriented neural simulator (E.D. Lumer, unpublished documentation). Numerical integration of the differential equations for the membrane potentials and channel conductances was based on a forward exponential technique (MacGregor, 1987; Wilson and Bower, 1989), with a time step of 0.5 ms. Experimentation with smaller time steps confirmed the integration accuracy. The generation of noise and statistical distribution of model parameters was based on standard random-number generator routines (Press *et al.*, 1992). The simulations were carried out on a Sun Sparc 20 workstation equipped with 256 Mbytes of memory. The full version of the model required ~180 Mbytes of memory and ran at a rate of ~5 CPU s/time step.

## Results

In the first part of the results, the dynamic behavior emerging from the physiological and anatomical constraints incorporated in the simulations is characterized by the population-averaged activity at each level of the model. Next, we examine how certain physiological parameters affect synchronous oscillations. For this purpose, parameters such as synaptic strengths, inhibitory time constants and transmission delays are systematically varied. Finally, we investigate the structural parameters that underlie synchronous oscillations. Sets of connections which support reentrant activity along intra- and interregional dynamic loops are selectively removed and their influence on synchronous oscillations is examined.
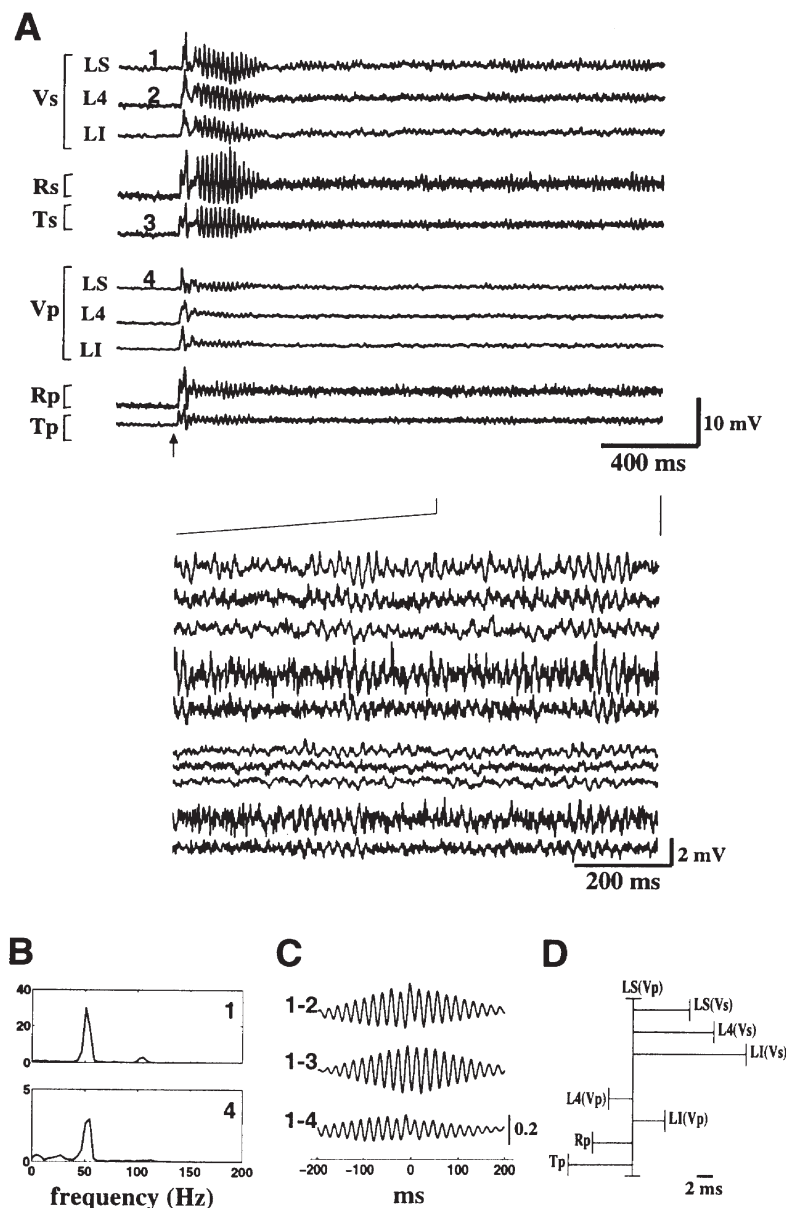
**Figure 2.** Oscillatory behavior of the thalamocortical model during visual stimulation. (A) (Upper plots) Shown from bottom to top are the population-averaged membrane potentials calculated in: Tp relays cells (1600 units), Rp cells (1600), excitatory cells in infragranular layer (6400), layer IV (6400), and supragranular layer (6400) of Vp, Ts relays cells (900), Rs cells (900), excitatory cells in infragranular layer (5400), layer IV (5400), and supragranular layer (5400) of Vs. The arrow at bottom left marks the stimulus onset. Note the enhanced amplitude of oscillations during the initial 300 ms after stimulus onset and before spike-rate adaptation sets in. (Lower plots) Same traces represented for a shorter time interval of 1 s during the tonic part of the network response. Epochs of enhanced population rhythmicity tended to occur simultaneously at all levels. (B) Power spectra of the population-averaged potentials in the supragranular layer of Vs (1) and of Vp (4) (unfiltered data). Peaks are centered at 52 Hz. (C) Cross-correlograms (CCs) computed between pairs of population-averaged membrane potentials at different thalamocortical levels. 1–2: CC between activities in supragranular layer and layer IV of Vs; 1–3: CC between activities in supragranular layer of Vs and in Ts; 1–4: CC between activities in supragranular layers of Vs and Vp. The initial transient response following stimulus onset was not included in these calculations. (D) Summary of time lags of activities at levels of the system with respect to activity in the supragranular layer of Vp. Time lags, measured as the zero-offset of the central peak in the CCs, varied between 4 ms or less (intracortical), and 4–14 ms (corticocortical and thalamocortical).

### Emergence of Multilevel Synchronous Oscillations

Figure 2 presents a typical example of population-averaged membrane potentials in the presence of the moving stimulus described in Materials and Methods. These population-averaged traces, computed independently at each thalamic and cortical level of the model, exhibit joint epochs of enhanced rhythmic activity (Fig. 2a). Note that model parameters underlying these synchronous oscillations were established *a priori* on the basis of experimental data and were not tuned to obtain any particular dynamic behavior. Thus, such sporadic episodes of fast oscillations are an emergent feature of the anatomical connectivity of the model and of the physiological properties of its units. The irregular occurrence of these oscillatory episodes (see also Fig. 10) is reminiscent of the phenomenon of intermittency that has been described in a number of nonlinear systems (Schuster, 1988).

Power spectra of the population-averaged activity traces were calculated to determine the main oscillation frequencies. They

**Figure 3.** Coherence between activities recorded at different spatial locations along the cortical surface. (Upper left) Population-averaged potentials were calculated from 10 × 5 patches slid along a horizontal line in the supragranular layer of Vs. (Lower left) Cross-correlograms (CCs) between averaged activities in patches separated by different distances. Disjoint populations of cells were used in each patch. 1–1′: Same location; 1–2: Adjacent 10 × 5 patches; 1–3: Maximally separated patches, given the wrap around connectivity in VS maps. This maximal separation corresponds to a physical distance of ~3–4 mm. Note that the central peaks all occur with near-zero phase lags. (Lower right) The amplitude of central peaks is plotted as a function of spatial separation, measured in number of cortical elements.

demonstrate the presence of prominent oscillations around 50 Hz in the response to visual stimuli (Fig. 2b). These power spectra are in qualitative agreement with those reported in the experimental literature (Eckhorn *et al.*, 1988; Gray *et al.*, 1992; Frien *et al.*, 1994). In order to assess the phase relationships between the neural activities at different thalamocortical levels, we computed the cross-correlogram of population-averaged membrane potentials in pairs of disjoint populations of neurons based on 1.5 s long recordings during sustained visual stimulation (Fig. 2c). This analysis established that populations of neurons at different levels were phase-locked, with time lags ranging from 0–4 ms (intraareal) to 4–14 ms (corticothalamic and corticocortical) (Fig. 2d).

The synchronization of fast rhythms within a cortical area has been shown to be spatially limited, being generally confined within a column and among closely located sites (Gray and Singer, 1989; Murthy and Fetz, 1992; Steriade *et al.*, 1996a). Activities measured at similar depths but different spatial locations in the cat cortex could synchronize with near-zero time lags, although their coherence was found to decrease with distance, becoming substantially weaker over 5 mm of separation measured tangentially along the cortex (Steriade *et al.*, 1996a). To compare the behavior of the model with these experimental findings, we measured the synchronization between averaged activities in spatially separated pools of neurons sampled from the supragranular layer of Vs. Consistent with the neurophysiological data from the cat, the coherence of fast rhythms was found to decrease gradually with spatial separation, becoming negligible at distances along the modeled cortical surface equivalent to 3–4 mm. Synchronization between different sites within the supragranular layers occurred with near-zero phase lags (Fig. 3). Similar coherence profiles were also observed in the primary cortical area (Vp).

## Physiological Parameters Affecting Synchronous Oscillations

In order systematically to explore the sensitivity of coherent firing regimes to certain physiological and anatomical properties of the circuitry, we used a scaled-down system which consisted of a single cortical area and associated thalamic structure, with maps of 10 × 10 elements at each level. The connectivity in the reduced model was similar to that generated in parts of the original system, for instance in a central 10 × 10 area of Ts, Rs and a single selectivity of Vs, with two exceptions: the profile of inhibitory connections within each cortical layer of the reduced model was rescaled to compensate for the loss of inhibitory inputs from competing selectivities; and the reference synaptic strengths were also doubled to account for a loss of synaptic connections originating from outside the 10 × 10 areas. Extrinsic thalamocortical activation was achieved in this reduced model by applying a Poissonian noise (amplitude = 10, rate = 0.2 kHz) independently to the excitatory channel of each thalamic unit.

As shown in Figure 4, the population-averaged response of this network with nominal parameters was qualitatively similar to that recorded in the extended model. Once again, synchronous oscillations emerged at all levels, with a slightly increased frequency of 56 Hz as compared with the original system.

### Synaptic Strengths

Synaptic strengths determine the efficacy of the interactions within the system, and they should therefore affect the emergence of fast rhythms. Generalized changes in synaptic strengths are likely to occur over long time windows in the course of development and learning, and over shorter time scales as a result of brainstem neuromodulatory influences. In the model, we tested the effect of synaptic efficacy on rhythmo-genesis by scaling all the synaptic strengths (i.e. both excitatory and inhibitory) by the same amount. Figure 5 compares the population-averaged potentials of a representative neuronal population in networks with strengths as stated earlier or with strengths decreased by either 25 or 50%. As shown in averaged membrane potential traces and in associated raster diagrams, as the synaptic strengths decrease in the thalamocortical circuit, oscillations exhibit smaller amplitudes – i.e. fewer cells fire synchronously – before disappearing altogether. Power spectral analysis of the population-averaged traces revealed a progressive concentration of their energy in the higher frequency bands as the synaptic efficacies were increased. Because the recruitment of more cells into the collective firing dynamics can have an effect equivalent to that of increasing synaptic efficacies, these results also suggest that a wide range of oscillatory frequencies can be expressed in the same system as different sensory stimuli or intrinsic states elicit responses in neural populations of varying sizes.

### Fast Inhibitory Time Constants

Widespread inhibition provides an efficient mechanism for synchronizing networks that have both excitatory and inhibitory cells. The activation of inhibitory cells can produce a postsynaptic hyperpolarization (IPSP) of target neurons followed by a rebound of synchronous firing in excitatory–inhibitory circuits (Cobb *et al.*, 1995). The repetition of this cycle leads to oscillations, at frequencies which should depend on the duration of individual IPSPs. Such a mechanism has often been invoked to account for cortical and thalamic rhythmicity (Bush and Douglas, 1991; Wilson and Bower, 1992). To test its potency in
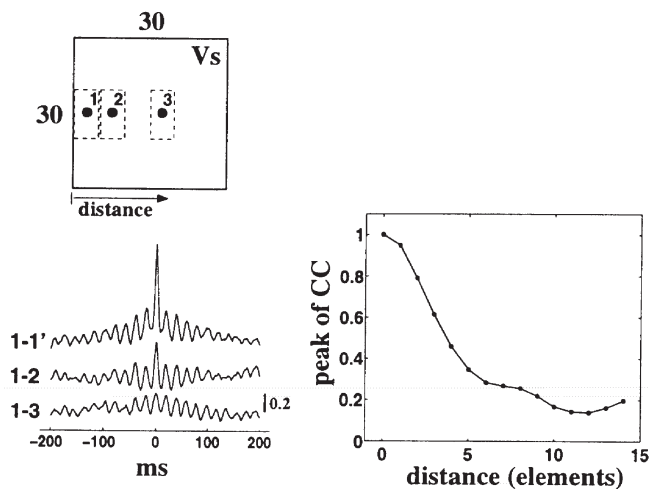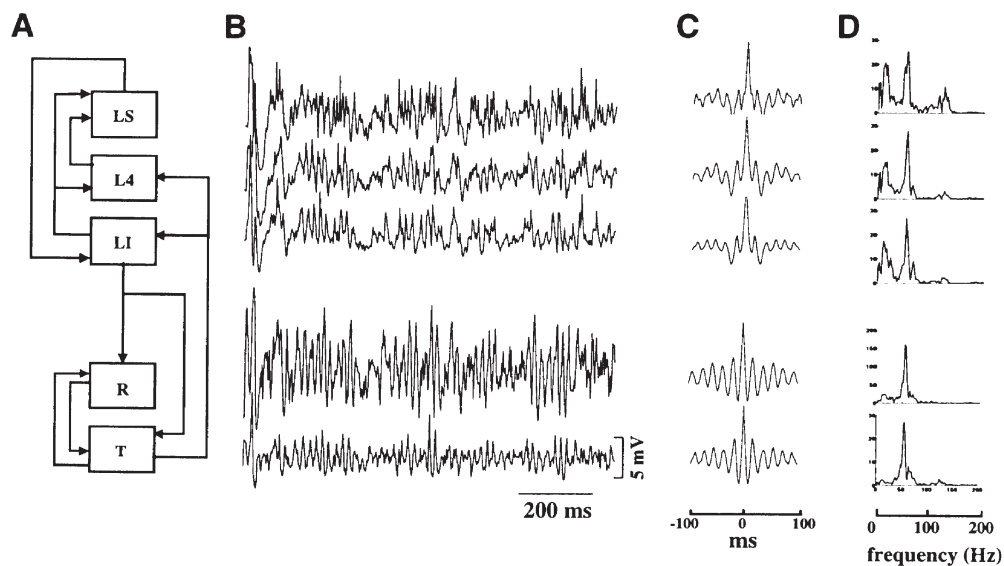
**Figure 4.** Fast activities in a reduced thalamocortical model. (*A*) Schematic layout of the 'vertical' connectivity in a system composed of a single cortical area and its associated thalamic structures (see main text). (*B*) Population-averaged voltage traces at five different levels of the model (i.e. thalamocortical, reticular thalamic and the three cortical subdivisions. (*C*) Autocorrelograms based on these traces reveal network oscillations at every level. (*D*) Power spectra analysis of these traces indicate that the oscillations occur mainly at a frequency of ~56 Hz.
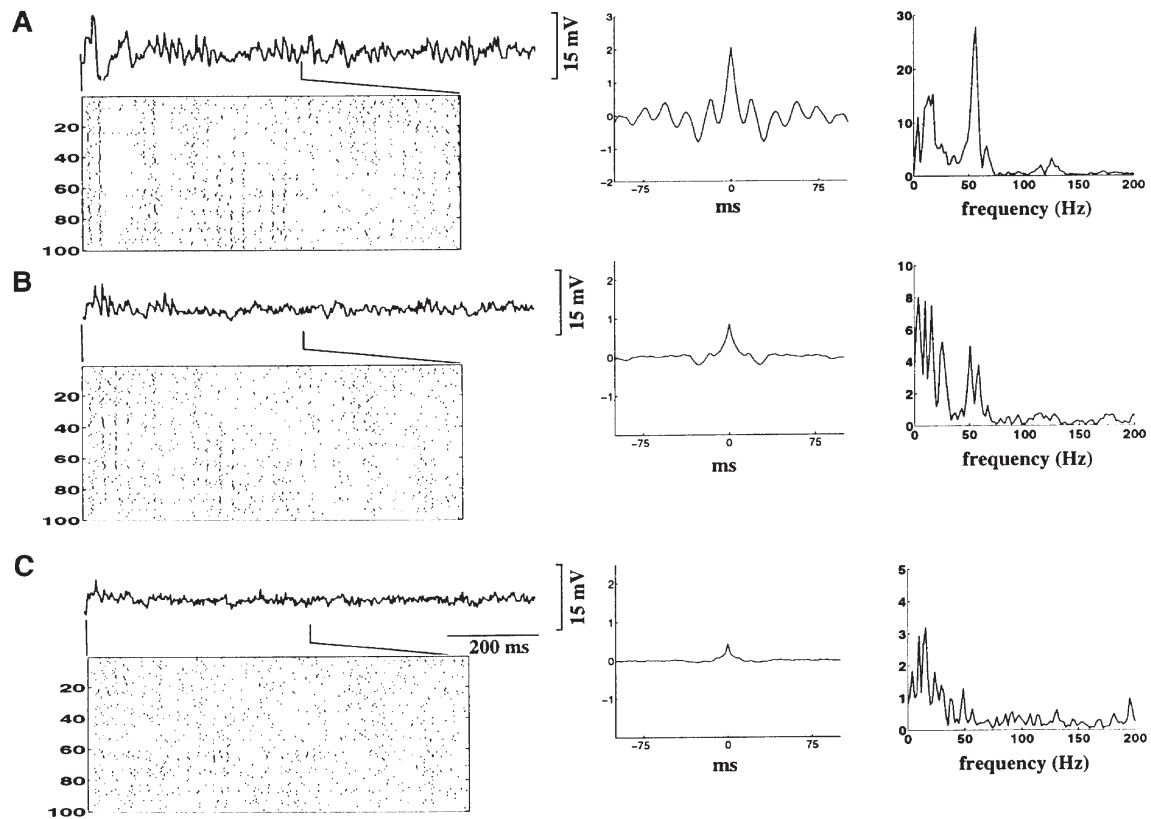


**Figure 5.** Effect of synaptic strengths on synchronous and oscillatory behavior. The reduced thalamocortical model was run with nominal synaptic strengths (*A*), and with strengths reduced by 25% (*B*) and 50% (*C*). In each case, the population-averaged intracellular voltage in layer IV is shown for a period of 1 s after stimulation onset. Raster plots of 100 excitatory units are shown over the first 500 ms of this period. Note the gradual loss of synchrony as synaptic efficacies decrease. Autocorrelograms of the population-averaged potentials are shown on the right side of the figure. They confirm the dependence of synchrony (central peak) and rhythmicity (side peaks) on synaptic efficacies. Corresponding power spectra are shown on the far right.
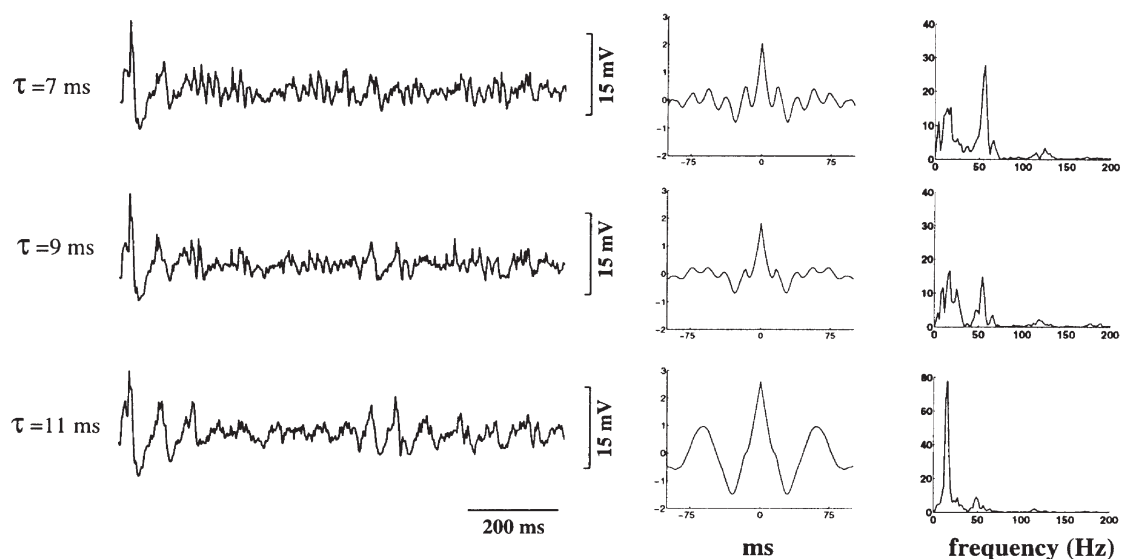
**Figure 6.** Effect of inhibition on oscillatory behavior. Population-averaged voltage traces in layer IV are shown for three values of the decay time constant ($\tau_2$) of fast inhibition, namely of 7 ms (nominal), 9 ms and 11 ms. Corresponding autocorrelograms and power spectra are shown in the central and right column respectively. Note in the autocorrelograms the attenuation of side peaks corresponding to fast 56 Hz rhythms as the time course of inhibition increases. For increasing inhibitory time courses, the concentration of spectral energy shifts from a 40–60 Hz band to a 15–20 Hz band.
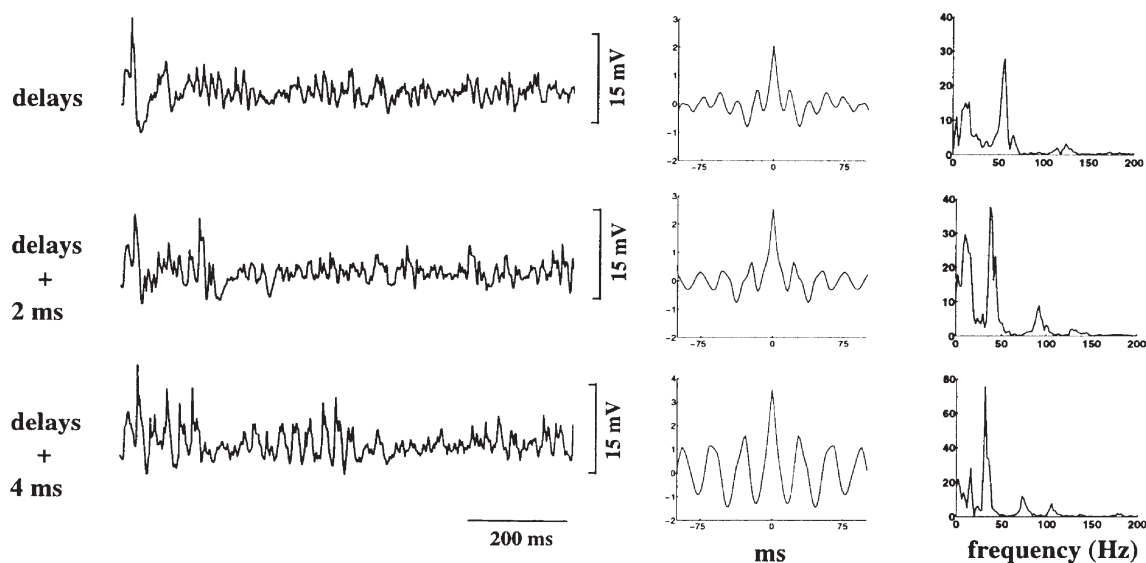


**Figure 7.** Effect of transmission delays on oscillatory behavior. Population-averaged traces in layer IV and their associated autocorrelograms and power spectra were computed for transmission delays at nominal levels (top) and at levels increased uniformly by either 2 ms (middle) or 4 ms (bottom). As indicated by the analysis of the autocorrelograms and power-spectra measurements, oscillatory frequencies gradually decrease for increasing values of the transmission delays (top = 56 Hz, middle = 46 Hz, bottom = 36 Hz).

the present context, we increased the open channel time for the Cl⁻-mediated inhibition (GABA$_A$) while decreasing its peak conductance so as to maintain constant the net inhibitory current associated with individual IPSPs. This procedure allowed us to compare the neural dynamics in networks with similar levels of excitability. As the inhibitory decay time was increased, the system shifted gradually from a fast oscillatory regime, with most of the spectral energy in the 40–60 Hz frequency band, to a slower rhythmicity in the 15–20 Hz range. These results, which are summarized in Figure 6, confirm the importance of inhibition in generating oscillatory behavior.

*Transmission Delays*
Axonal transmission delays affect neural network interactions without changing the intrinsic input–output properties of individual neurons. Thus, they represent a simple way to test whether the observed oscillations are a network property. Population-averaged potentials were compared for uniform increments of mean transmission delays applied throughout the modeled circuitry. Increases of delays limited to a few selected pathways are considered later. As shown in Figure 7, increasing the mean transmission delays resulted in a gradual decrease in the value of the peak oscillatory frequencies. Thus, these
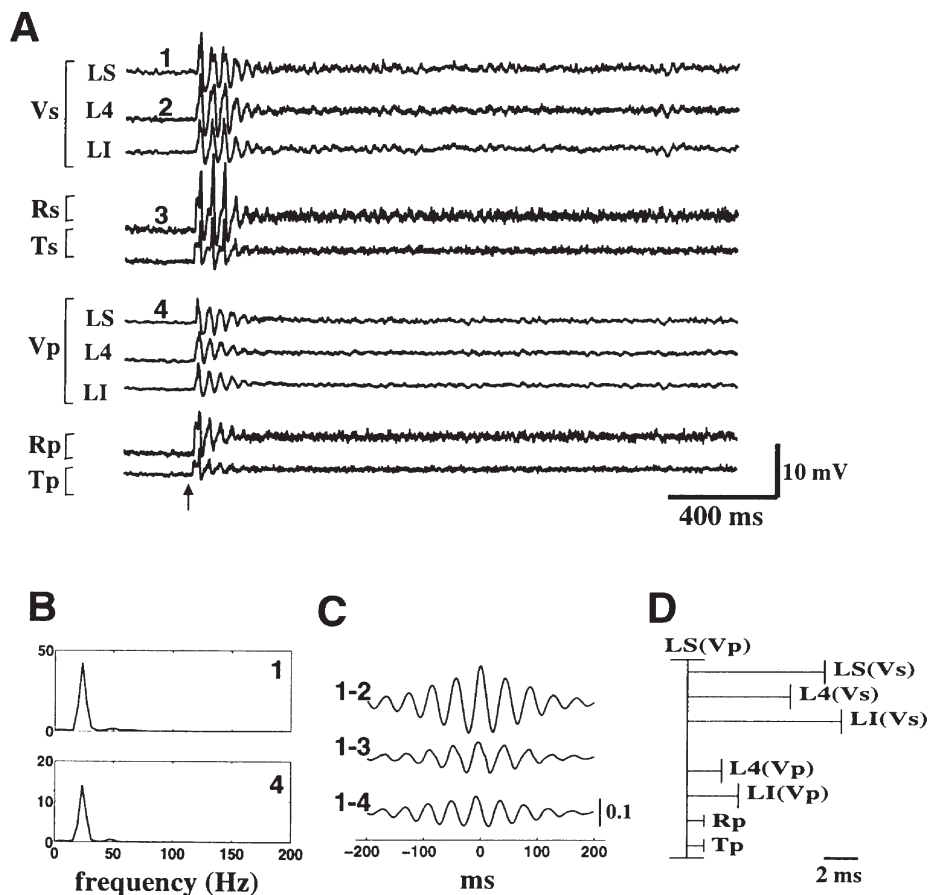
**Figure 8.** Oscillatory behavior of the extended thalamocortical model with shorter transmission delays. (*A*) Population-averaged membrane potentials at all levels of the model. (*B*) Power spectra reveal a dominant frequency at around 25 Hz. (*C*) Cross-correlograms calculated between disjoint populations of neurons. (*D*) Summary of the time lags of distributed activities with respect to the activity in the supragranular layer of Vp. Note the tight synchronization within Vp and between Vp and Tp.

experiments further suggest a network origin for the observed gamma-oscillations. The respective contributions of local and long-range processes are examined in the next section.

We also tested the effect of decreasing the comparatively longer delays that were introduced in certain sets of connections to account for disynaptic pathways not included in the model (see Materials and Methods). In this test, mean transmission delays from infragranular layer to layer IV were decreased to 2 ms; the mean delays from Vs to Vp and from cortex to thalamus were set to 3 ms. The results of these changes are shown in Figure 8. As illustrated in the figure, the introduction of shorter delays did not prevent oscillations from arising at all levels of the system (Fig. 8*a*), although their main frequencies were moved to a lower range, 20–30 Hz (Fig. 8*b*). The degree of synchronization in the system was also affected by these modifications: phase lags dropped from 0–4 ms to 0–3 ms (intra- and interlaminar), from 4–8 ms to 1 ms (corticothalamic) and from 7–14 ms to 6–9 ms (interareal) (Fig. 8*c–d*).

### Structural Parameters Affecting Synchronous Oscillations

The anatomical substrate of fast synchronous oscillations in cortical and thalamic circuits was studied in a series of simulated lesion experiments which selectively removed certain pathways from the thalamocortical connectivity.

### Interareal Loop

The full thalamocortical model (i.e. including two cortical areas and associated thalamic sectors) was used to assess the influence of the forward and backward corticocortical interactions on the spread of fast rhythms. The removal of backward projections from Vs to Vp in effect isolates the primary thalamocortical areas from any 'extrastriate' influence. As shown in Figure 9*a*, this manipulation does not prevent the emergence of synchronous oscillations at gamma frequencies in Vp and Tp. The removal of the forward projections from Vp to Vs, on the other hand, had a dramatic influence on the response found in the secondary area. Indeed, the lesion led to a disappearance of the fast synchronous rhythms within and between Ts and Vs (Fig. 9*b*), as well as to a decrease of the level of activity in Vs (data not shown). This result is consistent with the experimental observations that the lesioning of striate cortex typically has a greater impact on the activation in extrastriate areas than that on striate cortex resulting from a blockade of the activity in extrastriate cortex (Girard and Bullier, 1989; Girard *et al.*, 1991). In the model, these differential responses to lesions reflected the asymmetric connectivity between primary and secondary areas: whereas the forward projections from Vp to Vs represented a major source of extrinsic activation in Vs, the backward projections from Vs to Vp had only a modulatory (voltage-dependent) influence in the latter area.
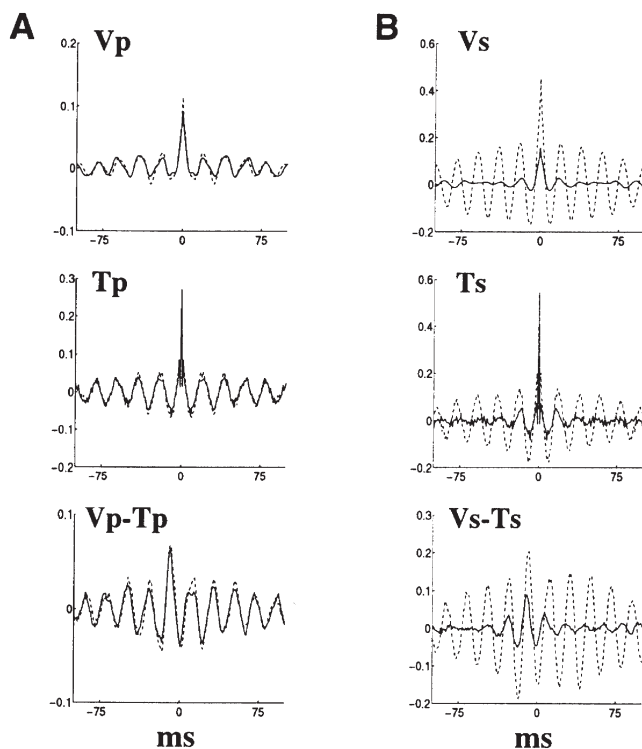
**A**

Vp

Tp

Vp-Tp

ms

**B**

Vs

Ts

Vs-Ts

ms

**Figure 9.** Lesion of backward or forward corticocortical projections. (*A*) Lesioning of backward corticocortical projections did not prevent oscillations in Vp and Tp. (Upper plot) Autocorrelogram of the population-averaged voltage in supragranular layer of Vp. (Middle plot) Autocorrelogram of the population-averaged voltage in Tp. (Bottom plot) Cross-correlogram between averaged voltages in supragranular layer of Vp and in Tp. The solid lines correspond to the lesioned system. These should be compared with the equivalent correlograms in the unaltered system (dashed lines). (*B*) Lesioning the forward corticocortical projections led to a dramatic decrease of coherence in Vs and Ts. (Upper plot) Autocorrelogram of the population-averaged voltage in supragranular layer of Vs. (Middle plot) Autocorrelogram of the population-averaged voltage in Ts. (Lower plot) Cross-correlogram between averaged voltages in supragranular layer of Vs and in Ts. The solid lines correspond to the lesioned system. Dashed lines represent responses in the unaltered system.

*Horizontal Intralaminar Loops*

Population-averaged voltage traces indicated that coherent activity could be observed at topographically distant cortical sites. The extended model (i.e. with two cortical areas and associated thalamic sectors) was used to test the influence of long-range excitatory projections that run parallel to the cortical surface on the synchronization of spatially segregated activity within a given brain region. Horizontal excitatory projections were removed from the intracortical circuitry in both Vp and Vs. The responses of neurons in a representative population, in this case the cells in supragranular layer of Vs, were then compared to those found in the unaltered model. The removal of horizontal projections was accompanied by a disappearance both of fast rhythms and of coherent activity between different spatial locations (data not shown). These results confirm the key role played by horizontal connections in the tangential synchronization of cortical activity.

*Interruption of Interlaminar and Thalamocortical Loops.*

Figure 10*b* shows the cortical and thalamic population-averaged activities in the system when corticothalamic and interlaminar backprojections are eliminated. The corresponding activities in the intact system are reproduced in Figure 10*a* for comparison

(these and the remaining experiments were performed in the reduced model). As shown in the figures, the removal of back projections leads to the disappearance of fast oscillations in the population-averaged potentials of both cortical and thalamic cells. However, a closer look at the firing patterns in cortex reveals a significant degree of intracortical synchronization, which is most prominent within the supragranular layer (Fig. 11). The presence of internally generated synchrony was measured here by computing the cross-correlograms between cumulated spike counts in non-overlapping populations and subtracting the shift predictor. These results suggest that the sequence of convergent–divergent projections along the forward visual pathway, combined with a horizontal coupling at each cortical level, induces a gradual build-up of synchrony as one moves from the periphery to the cortical surface. This explains the prominence of synchronous volleys among supragranular cells. However, in the absence of backprojections, reentry of these synchronous volleys into lower stages of the forward processing sequence cannot occur. That such reentry along corticocortical and corticothalamic projections is key for the generation of fast rhythms is demonstrated in the following experiments.

*Interlaminar Loop*

One consequence of restoring the interlaminar backprojections from the supragranular to infragranular layer in the reduced model is the emergence of fast intracortical oscillations in the 60 Hz frequency range. This is illustrated in Figure 10*c*, which should be compared to Figures 10*a* and 10*b*. Examination of the activity patterns in the cortex and in the thalamus indicates that fast synchronous rhythms can be generated strictly as a by-product of intra- and interlaminar cortical interactions, in the absence of sustained thalamic oscillations which require corticothalamic projections. In the absence of corticothalamic projections, different lesions which disrupted the interlaminar loops were equally effective in preventing oscillatory behavior: fast activities were suppressed either by removing the back-projections from supra- to infragranular layer (see Fig. 10*b*) or by removing the forward projections from the latter to layer IV and to the supragranular layer (data not shown).

*Thalamocortical Loop*

The above data do not imply that the ability to generate fast oscillations is an exclusive property of intracortical circuits. In addition to these circuits, a good candidate for the generation of sustained oscillations is the thalamocortical loop. To test this possibility, we considered the activity in a network in which the intracortical loop was disrupted but the corticothalamic pathways were preserved (Fig. 10*d*). In the presence of cortico-thalamic projections, fast synchronous oscillations could be seen both in cortex and thalamus. Analysis of the autocorrelograms associated with the population-averaged voltage traces indicated an oscillatory frequency of 45 Hz. This frequency could be varied by increasing or decreasing the transmission delays along either the corticothalamic or the thalamocortical pathways. On the other hand, changes of transmission delays within horizontal cortical networks left this frequency of oscillation unchanged. Thus, these manipulations further link the observed rhythmicity to the synchronous activation of a polysynaptic corticothalamo-cortical loop.

We also used the simulations to test the possible influences of the RT nucleus, which occupies a strategic position in thalamo-cortical circuits. This was done by removing the reticulothalamic
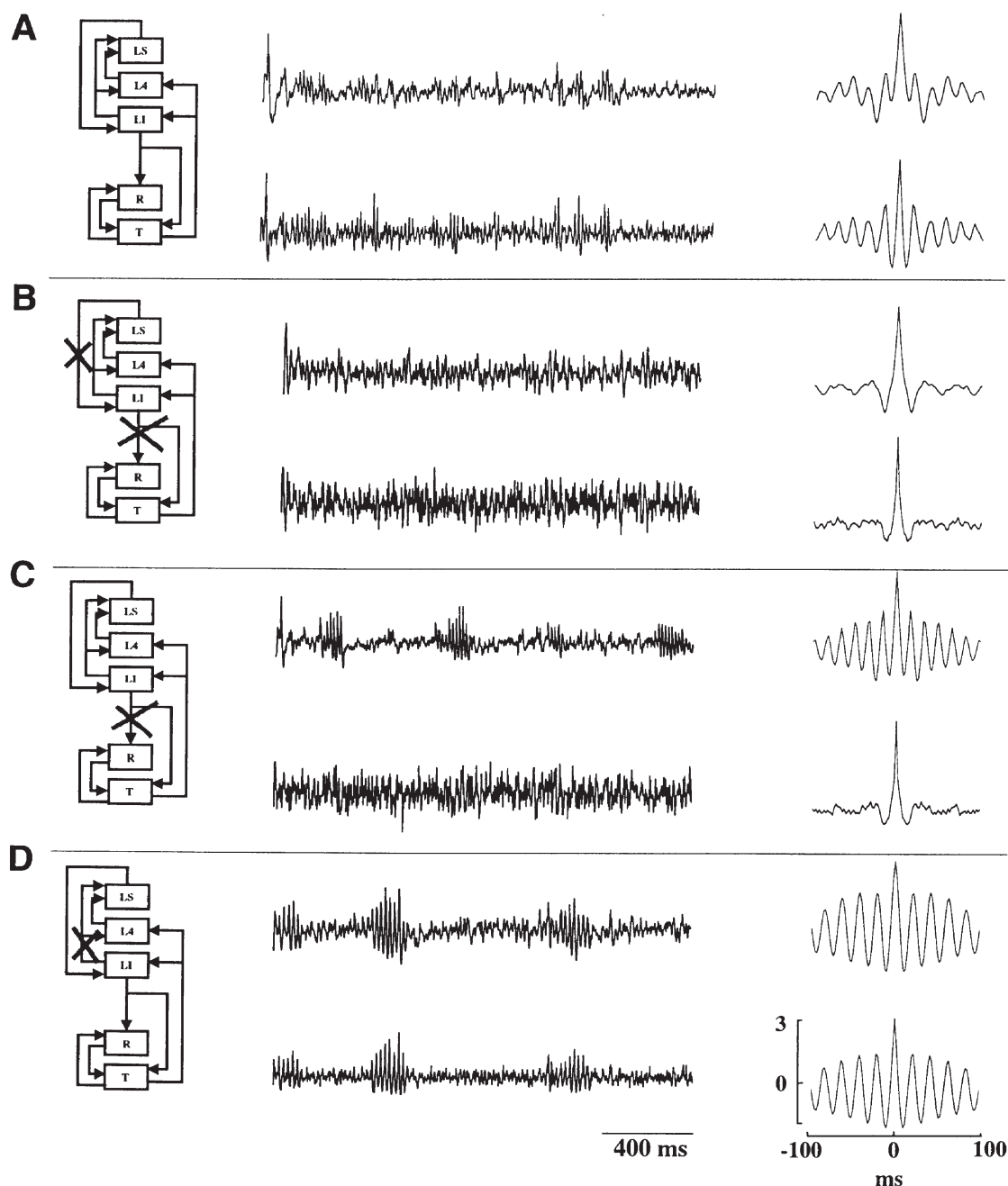
**Figure 10.** Lesion experiments in a reduced thalamocortical model. Alterations of the connectivity are shown in the left column. The central column contains population-averaged voltage traces at a thalamic (T) and cortical level (layer IV). The corresponding autocorrelograms are shown on the far right. (*A*) Unaltered thalamocortical model. (*B*) Model in which backward intracortical and corticothalamic projections were removed. Notice the disappearance of fast activities. (*C*) Restoring the interlaminar cortical loop alone leads to fast oscillations in cortex in the 60 Hz frequency range. (*D*) Thalamocortical loop alone. Sustained synchronous oscillations at 45 Hz span over the cortical depth and thalamus.

inhibitory projections. To allow a meaningful comparison between the effects of this manipulation and the original behavior, the local inhibition of relay cells was strengthened to compensate for the loss of RT inhibition. The removal of reticulothalamic projections led to a substantial decrease of synchronous oscillations both in cortex and thalamus (Fig. 12). Selective lesions of the thalamoreticular projections also abolished the oscillations, indicating that in the model the thalamoreticular projections play a prominent role in driving the

RT nucleus into synchrony (data not shown). The synchronization of RT cells due to direct corticoreticular and indirect cortico-thalamo-reticular activations results in turn in the simultaneous firing of thalamic relay cells. Taken together, these results confirm the importance of cortico-reticulo-thalamic interactions in generating sustained oscillations in the thalamocortical model. However, our simulations cannot rule out the possibility that corticothalamic influences are mediated directly by local-circuit IPSPs. Indeed, we found that with
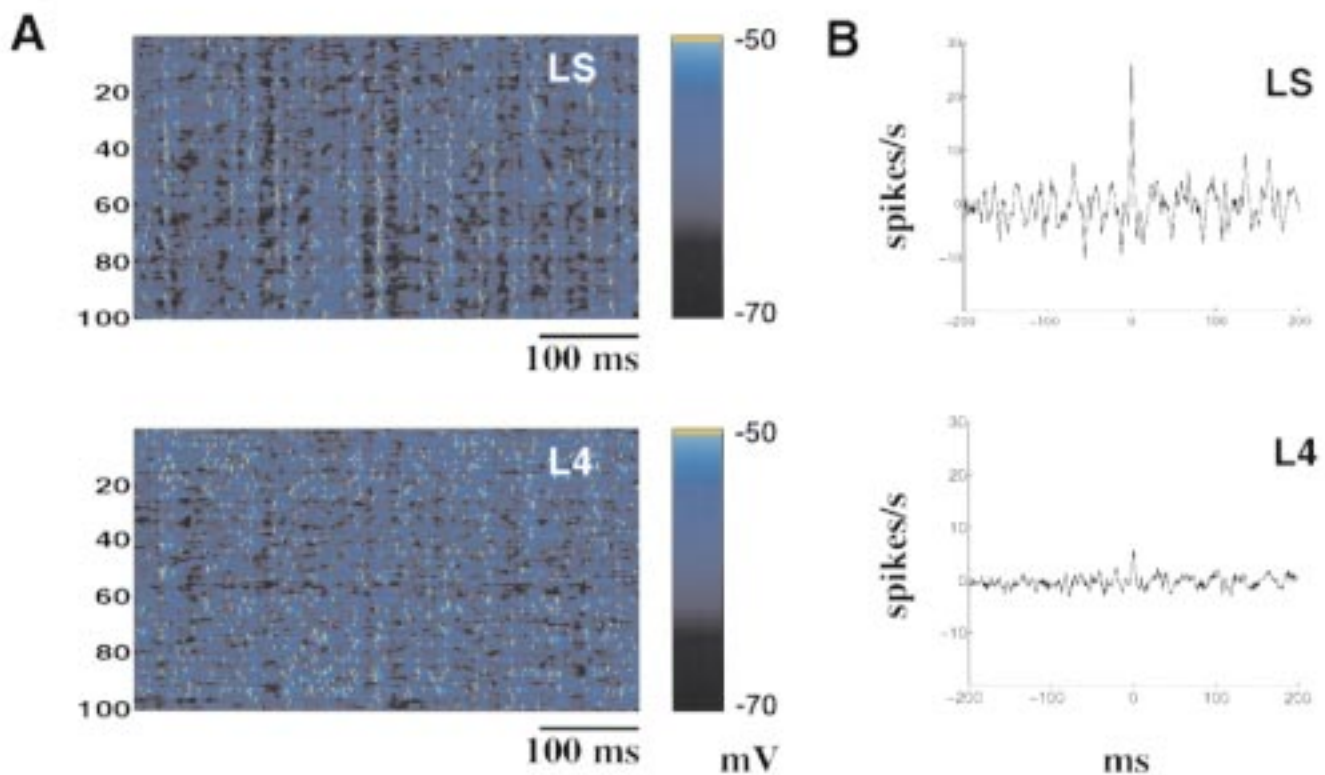
**Figure 11.** Synchronization of activity due to forward and intralaminar projections. The connectivity was as in Figure 10*B*. (*A*) Membrane potential plots of 100 units in layer IV (L4) and 100 units in supragranular layer (LS) are shown over a period of 500 ms. Firing synchrony among supragranular cells can be readily seen in these plots (spikes shown in yellow). (*B*) The enhanced synchronization in LS is confirmed by computing cross-correlograms of spiking activity as follows: excitatory cells in LS (respectively L4) were divided in two non-overlapping populations with a 100 units each; the cumulated spike counts were calculated for each population and cross-correlated against each other (bin = 1 ms). The resulting cross-correlograms were plotted after subtraction of a shift predictor and normalization by the number of units.

different model parameters the synchronization of relay cells could also be supported by local inhibition, even in the absence of reticulo-thalamic projections.

## Discussion

We have presented a large-scale computer model which incorporates the basic structural and physiological components of thalamocortical systems. The model incorporates both the dynamic constraints due to the layered structure and long-range connectivity of the thalamocortical system, as well as physiological properties of individual neurons and local synaptic networks. This distinguishes it from models that emphasize the biophysical properties of single neurons but are chiefly concerned with the functioning of the local cortical (Bush and Douglas, 1991; Douglas *et al.*, 1991; Douglas *et al.*, 1995; Somers *et al.*, 1995; Maex and Orban, 1996) or thalamic circuitry (Golomb *et al.*, 1994; Destexhe *et al.*, 1994). On the other hand, this model differs from other large-scale simulations of cortical functioning (see e.g. Sporns *et al.*, 1991; Wörgötter and Koch, 1991; Wilson and Bower, 1992; Tononi *et al.*, 1992; Nowlan and Sejnowski, 1995; Stemmler *et al.*, 1995), in that it explicitly simulates the layered cortical structure, the long-range intralaminar and the intracolumnar connectivity, the laminar specificity of forward and backward corticocortical projections, and the thalamocortical and thalamoreticular loops. By allowing us to examine the effects of selective anatomic manipulations on fast rhythms, the present model prompts the suggestion that thalamocortical systems are organized in terms of a number of prototypical 'macro-circuits' defined by their patterns of connectivity and by their dynamic properties. Some of these macro-circuits are: (i) horizontal patchy networks within each layer of cortex; (ii) interlaminar cortical loops; (iii) interareal corticocortical loops; and (iv) thalamocortical loops realized through the RT complex.

Simulations based on this model have been used to investigate in detail the influences on synchronous rhythms of physiological parameters such as synaptic strength, time constant of inhibition, transmission delays, and of structural parameters affecting intralaminar, interlaminar, thalamocortical and thalamoreticular macro-circuits. This analysis has led to several findings concerning the specific role of each of these macro-circuits: (i) in addition to the known oscillatory influences imposed by local cortical networks, the emergence of high frequencies in population-averaged activities was found to depend critically on the dynamics of polysynaptic loops; (ii) an interlaminar cortical loop provided a high-gain amplification mechanism that drove the local cortical networks into an oscillatory regime, even in the absence of thalamic rhythmicity; (iii) in addition to these circuits, a corticothalamocortical loop involving the RT complex could induce synchronous oscillations at thalamic and cortical levels; (iv) horizontal networks within each cortical layers as well as forward and backward interareal projections contributed to the spread of these coherent oscillations over extended cortical territories.

In what follows, we reexamine the neurophysiological data on the generation of fast thalamocortical rhythms in the light of these new results. We consider in turn the role of cortical inhibition, the role of network versus cellular mechanisms of
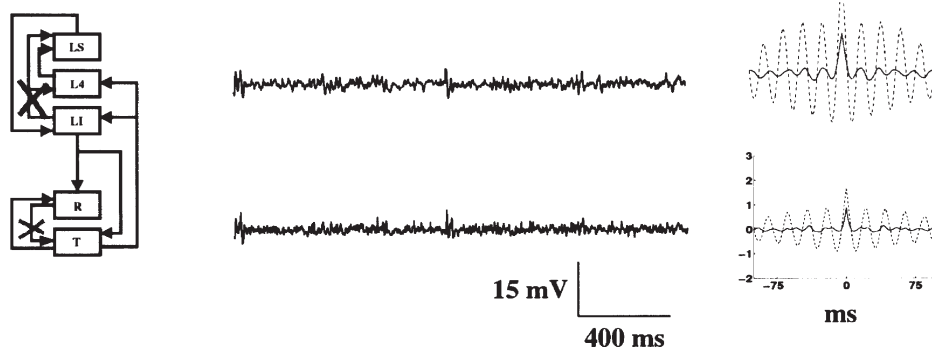
**Figure 12.** Influence of the reticular thalamic nucleus. The organization of the figure is similar to Figure 10*D*, which tied the activation of a thalamocortical loop to the onset of fast rhythms. In the present figure, an additional lesion was introduced at the level of the reticulothalamic pathway. The efficacy of thalamic inhibition due to local interneurons was concurrently increased to maintain constant the mean firing rate of relay cells, at 51 spikes/s. The blockade of RT inhibition drastically impaired the ability of the thalamocortical loop to generate fast oscillations. For reference, the autocorrelograms of averaged activities in T and layer IV are also represented for the model with intact reticulothalamic projections, using dashed lines.

oscillations, the influence of intracortical loops, that of thalamocortical and thalamoreticular loops, and finally the possible significance of other factors that have not yet been included in the present model.

### Role of Cortical Inhibition

That networks of simplified cortical neurons with excitatory and inhibitory couplings have a propensity to oscillate in the gamma range was proposed long ago. Previous modeling studies demonstrating this behavior have emphasized the importance of inhibitory time constants in shaping periodic activity (Traub *et al.*, 1989; Wilson and Bower, 1992). Recent experiments performed in slices of rat hippocampus and neocortex have confirmed that networks of inhibitory interneurons can generate fast oscillations that can entrain synchronous pyramidal cells discharges (Whittington *et al.*, 1995). The principal oscillatory frequency was found to decrease monotonically as the decay time constant of fast (GABA$_A$-mediated) IPSCs increased. In the present simulations, the dominant peak frequencies in the thalamocortical oscillations did not shift gradually in response to incremental changes of the fast inhibitory decay time. Instead, the system dynamics evolved from a fast oscillatory regime, with most of the spectral energy in the 40–60 Hz frequency band, to a slower rhythmicity in the 15–20 Hz range, as the inhibitory decay time was increased. Strong oscillations in intermediary frequency bands (20–40 Hz) were not observed in the course of this manipulation. This apparent discrepancy between the behavior of the model and that of isolated cortical networks may result from the influences of long-range interactions in the intact thalamocortical system. Our simulations predict that, in addition to local inhibitory networks, thalamocortical loops also tend to oscillate in the 40 Hz range. The oscillatory dynamics thus reflects the combined influences of these two systems, which can be either mutually reinforcing or mutually exclusive. For small increases of the GABA$_A$ decay time constants, thalamocortical loops maintain the system in a regime dominated by high-frequency oscillations. As the decay time constant increases, the system dynamics becomes dominated by lower oscillatory frequencies that are primarily determined by inhibitory network interactions.

A distinctive feature of the present model in its treatment of cortical inhibition was the presence of two distinct populations of inhibitory cells that activated fast and slow hyperpolarizing channels respectively. GABA$_A$-mediated fast inhibition extended horizontally within each layer of the cortex, while cells located in the supragranular layer exerted a slow GABA$_B$-mediated inhibitory control over a narrow cylinder extending to all layers. The latter form of slow inhibition is consistent with the finding that slow IPSPs can be triggered in narrow columns running across all layers by stimulations located in supragranular layers (Kang *et al.*, 1994). This pattern of activation is also consistent with the anatomy of double-bouquet cells (Somogyi and Cowey, 1984). Early simulations indicated that the inhibitory effects mediated by these cells have a time constant and spatial extent such that they serve to balance the gradual amplification of activity taking place in interlaminar cortical loops.

### Network versus Cellular Mechanisms of Oscillations

Neurons throughout the nervous system are equipped with intrinsic properties that can cause them to oscillate in the gamma-frequency range. For instance, populations of sparsely spiny interneurons in cortical layer IV have been found to generate intrinsic 40 Hz oscillations when recorded *in vitro* (Llinás *et al.*, 1991). More recently, neurons in cat striate cortex that fire repetitive 40 Hz trains of short bursts when depolarized, have been characterized *in vivo* (McCormick and Gray, 1995). Similar properties have also been described when recording from neurons in peripheral sites such as the retina (Neuenschwander and Singer, 1996), in the thalamus, specific (Steriade *et al.*, 1991) and nonspecific (Steriade *et al.*, 1993), and in the RT nucleus (Pinault and Deschenes, 1992). These findings raise the possibility that the presence of neurons with intrinsic oscillatory capabilities at many levels of the thalamocortical system could play an important role in the generation of thalamocortical high-frequency oscillations. A striking result of the present simulations was that gamma rhythms could be produced even in the absence of intrinsic 40 Hz pacemaker mechanisms. These fast oscillations depended critically on the activation of intracortical circuits and thalamocortical loops, each with a natural frequency of oscillation in the gamma range. Thus, our simulations suggest that several network and cellular factors may cooperate to produce fast rhythms in thalamocortical systems. The properties of thalamocortical and intracortical circuits may be tuned to support oscillations at frequencies which are consistent with the natural frequencies of neuronal pacemakers.

### Intracortical Mechanisms of Synchronization

Synchronization of many cells is required to produce coherent fields that can be measured with extracellular and surface (e.g EEG, MEG) macro-electrodes. The respective contribution of cortical and subcortical structures in mediating such synchronization is hard to identify. By recording from opposite cortical hemispheres in the cat, Engel *et al.* (1991a) found synchronous oscillations in the gamma band between neurons at homotopic locations in opposite areas 17 during visual stimulation. These coherent oscillations were abolished by a section of the corpus callosum, thus suggesting that corticocortical connections can mediate the synchronization of fast rhythms. In addition, data obtained in slices of rat cortex indicated that even a limited portion of cortical circuits has a tendency to oscillate at gamma frequencies (Chagnac-Amital and Connors, 1989; Whittington *et al.*, 1995). The synchronizing influence of horizontal cortical connections is supported by recent studies in strabismic cats. In these studies, the loss of synchronization between neurons of area 17 responding to different eyes was correlated with the restriction of their horizontal connections to cells that responded to same eye (König *et al.*, 1993).

Simulations in the thalamocortical model exhibit a behavior that is consistent with these observations. Synchronous oscillations emerged in the simulated cortex even in the absence of thalamic rhythmicity. These coherent fast cortical rhythms were found to depend both on intra- and interlaminar projections. Disruption of the interlaminar loop abolished the oscillations and led to reduced firing levels, thus suggesting that the intracortical loop provides a high-gain amplification mechanism for driving the excitatory–inhibitory networks in an oscillatory regime. Without this amplification, a significant degree of synchrony was still found in the modeled cortex, with a preponderance of coherent activity in the superficial layers. Our simulations suggest that the ascending convergent–divergent sensory pathways, together with the horizontal intracortical projections, play a key role in generating this type of synchronization.

### Role of the Thalamocorticothalamic Loop and the RT Nucleus

In addition to corticocortical circuits, thalamocorticothalamic loops provide a possible substrate for the synchronization of neural activity. Evidence of mutual synchronizing influences between the cortex and the thalamus comes in part from recent studies in the cat. Relay cells of the LGN have been found to synchronize their firing in a stimulus-dependent manner (Sillito *et al.*, 1994). This synchronization was contingent on the extrinsic activation provided by the cortex. More recently, fast oscillations observed during states of focused attention were found to be synchronous between cortical and thalamic sites (Steriade *et al.*, 1996b). The strength of corticothalamic synchronization depended in this case on the presence of reciprocal connections between cortical and thalamic loci. Our simulations confirmed that the reciprocal interactions between the cortex and the thalamus are important in producing coherent patterns of activity. Moreover they allowed us to test the possible influences of the RT nucleus, which occupies a strategic position in thalamocortical circuits.

RT cells receive synaptic inputs from corticothalamic and thalamocortical axon collaterals, and, in return, RT cells project diffusely within the RT nucleus, as well as to most thalamic nuclei. On the basis of this connectivity, and given the presence of 40 Hz oscillations in specific thalamic nuclei, in the RT nucleus, and in the neocortex, it has been suggested that the generation of fast synchronous rhythms involves a form of thalamocortical resonance (Llinás and Paré, 1991; Llinás and Ribary, 1993). Corticothalamic volleys at 40 Hz would impinge upon RT cells, thus leading to a resonant 40 Hz synchronous activation of the RT nucleus. The inhibitory input from the RT nucleus would then sculpt the discharges of thalamocortical neurons. As a result, synchronous and oscillatory activity would reenter the cortex, where it would resonate with layer IV interneurons. Rather than involving the RT complex, synchronized corticothalamic volleys could directly excite the thalamocortical neurons which reenter the cortex a bit later, thus triggering a new cycle of synchronized firing. The regular repetition of this cycle would result in oscillations. This view is supported by the demonstration that, at 30–40 Hz, cortical stimulation leads to a marked enhancement of EPSPs in directly connected relay cells (Lindström and Wróbel, 1990). Finally, mixed mechanisms might operate in corticothalamic loops through both a direct activation of thalamocortical neurons and an indirect induction of RT-mediated and local-circuit couplings. The latter view is supported by our simulations. First, we observed that the discharge rates in thalamocortical cells were not significantly affected by the presence of corticothalamic projections, indicating that their net influence on thalamic relay cells – a product of direct excitation and indirect inhibition via the RT nucleus and local interneurons – is modulatory rather than excitatory. Furthermore, we found that the diffuse RT inhibition of thalamocortical neurons plays a critical role in sustaining synchronous oscillations in thalamocortical circuits. Finally, our simulations indicated that thalamic volleys impinging on the RT were important in driving that structure into synchrony.

### Other Factors Influencing Synchronization

Experimental measurements of the temporal correlations between activities in separate visual cortical areas have often revealed synchronous oscillations with zero phase lags (Engel *et al.*, 1991a,b; Nelson *et al.*, 1992; Singer, 1993; Munk *et al.*, 1995). However, most of these data pertain to pairs of areas located at similar levels along the visual hierarchy, either within the same hemisphere or across the two cerebral hemispheres. In contrast, less is known regarding the phase relationships between activities in cortical areas that are separated by several levels along the visual hierarchy (Engel *et al.*, 1991b; Frien *et al.*, 1994). Whereas areas located at the same hierarchical level tend to exhibit a symmetric (lateral) pattern of interconnectivity, areas separated by several levels are typically interconnected by projections with asymmetric patterns of laminar origin and termination (Felleman and Van Essen, 1991). This asymmetry between forward and backward connectivity was reflected in the anatomical organization of the model, and resulted in systematic time lags between the activity of the simulated primary and secondary area ranging from 6 to 14 ms, depending on the actual model parameters and recording depths considered (see Figs 2 and 8). Note, however, that several anatomical pathways which may significantly reduce these time lags were not included in the simulations. For example, we did not consider the possible coupling between RT sectors associated with the primary and secondary thalamocortical pathways. Corticothalamic projections arising in the primary visual area were restricted to the LGN, while in reality they also enter the LP-pulvinar which, in turn, projects to secondary visual areas

**Table 3**

Connectivity table of the thalamocortical model

| Source area | Layer | Cell type | Target area | Layer | Cell type | Synaptic channel | Arbor spread | | Max pr. of connection | Space constant |
|---|---|---|---|---|---|---|---|---|---|---|
| **Primary visual area** | | | | | | | | | | |
| *Horizontal intralaminar connections* | | | | | | | | | | |
| Vp | L4 | e (v) | Vp | L4 | e (v) | AMPA | 15 | 15 | 0.1 | 7.5 |
| Vp | L4 | e (v) | Vp | L4 | i (v) | AMPA | 15 | 15 | 0.1 | 7.5 |
| Vp | LS | e (v) | Vp | LS | e (v) | NMDA | 25 | 25 | 0.1 | 7.5 |
| Vp | LS | e (v) | Vp | LS | i (v) | AMPA | 25 | 25 | 0.1 | 7.5 |
| Vp | LI | e (v) | Vp | LI | e (v) | AMPA | 25 | 25 | 0.1 | 7.5 |
| Vp | LI | e (v) | Vp | LI | i (v) | AMPA | 25 | 25 | 0.1 | 7.5 |
| *Vertical interlaminar connections* | | | | | | | | | | |
| Vp | L4 | e (v) | Vp | LS | e (v) | AMPA | 5 | 5 | 1 | 7.5 |
| Vp | L4 | e (v) | Vp | LS | i (v) | AMPA | 5 | 5 | 1 | 7.5 |
| Vp | LS | e (v) | Vp | LI | e (v) | AMPA | 5 | 5 | 1 | 7.5 |
| Vp | LS | e (v) | Vp | LI | i (v) | AMPA | 5 | 5 | 1 | 7.5 |
| Vp | LI | e (v) | Vp | L4 | e (v) | AMPA | 5 | 5 | 1 | 7.5 |
| Vp | LI | e (v) | Vp | L4 | i (v) | AMPA | 5 | 5 | 1 | 7.5 |
| Vp | LI | e (v) | Vp | LS | e (v) | AMPA | 5 | 5 | 1 | 7.5 |
| Vp | LI | e (v) | Vp | LS | i (v) | AMPA | 5 | 5 | 1 | 7.5 |
| *Intracortical inhibitory connections* | | | | | | | | | | |
| Vp | L4 | i (v) | Vp | L4 | e (v) | $GABA_A$ | 5 | 5 | 0.15 | 7.5 |
| Vp | L4 | i (v) | Vp | L4 | e (h) | $GABA_A$ | 5 | 5 | 0.15 | 7.5 |
| Vp | L4 | i (v) | Vp | L4 | i (v) | $GABA_A$ | 5 | 5 | 0.15 | 7.5 |
| Vp | L4 | i (v) | Vp | L4 | i (h) | $GABA_A$ | 5 | 5 | 0.15 | 7.5 |
| Vp | LS | i (v) | Vp | LS | e (v) | $GABA_A$ | 15 | 15 | 0.05 | 7.5 |
| Vp | LS | i (v) | Vp | LS | e (h) | $GABA_A$ | 15 | 15 | 0.05 | 7.5 |
| Vp | LS | i (v) | Vp | LS | i (v) | $GABA_A$ | 15 | 15 | 0.05 | 7.5 |
| Vp | LS | i (v) | Vp | LS | i (h) | $GABA_A$ | 15 | 15 | 0.05 | 7.5 |
| Vp | LI | i (v) | Vp | LI | e (v) | $GABA_A$ | 15 | 15 | 0.05 | 7.5 |
| Vp | LI | i (v) | Vp | LI | e (h) | $GABA_A$ | 15 | 15 | 0.05 | 7.5 |
| Vp | LI | i (v) | Vp | LI | i (v) | $GABA_A$ | 15 | 15 | 0.05 | 7.5 |
| Vp | LI | i (v) | Vp | LI | i (h) | $GABA_A$ | 15 | 15 | 0.05 | 7.5 |
| Vp | LS | i (v) | Vp | LS | e (v) | $GABA_B$ | 2 | 2 | 0.25 | ∞ |
| Vp | LS | i (v) | Vp | L4 | e (v) | $GABA_B$ | 2 | 2 | 0.25 | ∞ |
| Vp | LS | i (v) | Vp | LI | e (v) | $GABA_B$ | 2 | 2 | 0.25 | ∞ |
| **Secondary visual area** | | | | | | | | | | |
| *Horizontal intralaminar connections* | | | | | | | | | | |
| Vs | L4 | e (v) | Vs | L4 | e (v) | AMPA | 15 | 15 | 0.1 | 7.5 |
| Vs | L4 | e (v) | VS | L4 | i (v) | AMPA | 15 | 15 | 0.1 | 7.5 |
| Vs | LS | e (v) | Vs | LS | e (v) | NMDA | 25 | 25 | 0.1 | 7.5 |
| Vs | LS | e (v) | Vs | LS | i (v) | AMPA | 25 | 25 | 0.1 | 7.5 |
| Vs | LI | e (v) | Vs | LI | e (v) | AMPA | 25 | 25 | 0.1 | 7.5 |
| Vs | LI | e (v) | Vs | LI | i (v) | AMPA | 25 | 25 | 0.1 | 7.5 |
| *Vertical interlaminar connections* | | | | | | | | | | |
| Vs | L4 | e (v) | Vs | LS | e (v) | AMPA | 5 | 5 | 1 | 7.5 |
| Vs | L4 | e (v) | Vs | LS | i (v) | AMPA | 5 | 5 | 1 | 7.5 |
| Vs | LS | e (v) | Vs | LI | e (v) | AMPA | 5 | 5 | 1 | 7.5 |
| Vs | LS | e (v) | Vs | LI | i (v) | AMPA | 5 | 5 | 1 | 7.5 |
| Vs | LI | e (v) | Vs | L4 | e (v) | AMPA | 5 | 5 | 1 | 7.5 |
| Vs | LI | e (v) | Vs | L4 | i (v) | AMPA | 5 | 5 | 1 | 7.5 |
| Vs | LI | e (v) | Vs | LS | e (v) | AMPA | 5 | 5 | 1 | 7.5 |
| Vs | LI | e (v) | Vs | LS | i (v) | AMPA | 5 | 5 | 1 | 7.5 |

**Table 3** – *continued*

| Source area | Layer | Cell type | Target area | Layer | Cell type | Synaptic channel | Arbor spread | | Max pr. of connection | Space constant |
|---|---|---|---|---|---|---|---|---|---|---|
| *Intracortical inhibitory connections* | | | | | | | | | | |
| Vs | L4 | i (v) | Vs | L4 | e (v) | GABA$_A$ | 5 | 5 | 0.15 | 7.5 |
| Vs | L4 | i (v) | Vs | L4 | e (h) | GABA$_A$ | 5 | 5 | 0.075 | 7.5 |
| Vs | L4 | i (v) | Vs | L4 | e (c) | GABA$_A$ | 5 | 5 | 0.075 | 7.5 |
| Vs | L4 | i (v) | Vs | L4 | i (v) | GABA$_A$ | 5 | 5 | 0.15 | 7.5 |
| Vs | L4 | i (v) | Vs | L4 | i (h) | GABA$_A$ | 5 | 5 | 0.075 | 7.5 |
| Vs | L4 | i (v) | Vs | L4 | i (c) | GABA$_A$ | 5 | 5 | 0.075 | 7.5 |
| Vs | LS | i (v) | Vs | LS | e (v) | GABA$_A$ | 15 | 15 | 0.05 | 7.5 |
| Vs | LS | i (v) | Vs | LS | e (h) | GABA$_A$ | 15 | 15 | 0.025 | 7.5 |
| Vs | LS | i (v) | Vs | LS | e (c) | GABA$_A$ | 15 | 15 | 0.025 | 7.5 |
| Vs | LS | i (v) | Vs | LS | i (v) | GABA$_A$ | 15 | 15 | 0.05 | 7.5 |
| Vs | LS | i (v) | Vs | LS | i (h) | GABA$_A$ | 15 | 15 | 0.025 | 7.5 |
| Vs | LS | i (v) | Vs | LS | i (c) | GABA$_A$ | 15 | 15 | 0.025 | 7.5 |
| Vs | LI | i (v) | Vs | LI | e (v) | GABA$_A$ | 15 | 15 | 0.05 | 7.5 |
| Vs | LI | i (v) | Vs | LI | e (h) | GABA$_A$ | 15 | 15 | 0.025 | 7.5 |
| Vs | LI | i (v) | Vs | LI | e (c) | GABA$_A$ | 15 | 15 | 0.025 | 7.5 |
| Vs | LI | i (v) | Vs | LI | i (v) | GABA$_A$ | 15 | 15 | 0.05 | 7.5 |
| Vs | LI | i (v) | Vs | LI | i (h) | GABA$_A$ | 15 | 15 | 0.025 | 7.5 |
| Vs | LI | i (v) | Vs | LI | i (c) | GABA$_A$ | 15 | 15 | 0.025 | 7.5 |
| Vs | LS | i (v) | Vs | LS | e (v) | GABA$_B$ | 2 | 2 | 0.50 | ∞ |
| Vs | LS | i (v) | Vs | L4 | e (v) | GABA$_B$ | 2 | 2 | 0.50 | ∞ |
| Vs | LS | i (v) | Vs | LI | e (v) | GABA$_B$ | 2 | 2 | 0.50 | ∞ |
| Interareal connections | | | | | | | | | | |
| *Forward interareal connections* | | | | | | | | | | |
| Vp | LS | e (v) | Vs | L4 | e (v) | AMPA | 19 | 3 | 0.8 | 7.5 |
| Vp | LS | e (v) | Vs | L4 | i (v) | AMPA | 19 | 3 | 0.8 | 7.5 |
| Vp | LS | e (h) | Vs | L4 | e (h) | AMPA | 3 | 19 | 0.8 | 7.5 |
| Vp | LS | e (h) | Vs | L4 | i (h) | AMPA | 3 | 19 | 0.8 | 7.5 |
| Vp | LS | e (v) | Vs | L4 | e (c) | AMPA | 9 | 3 | 0.8 | 7.5 |
| Vp | LS | e (v) | Vs | L4 | i (c) | AMPA | 9 | 3 | 0.8 | 7.5 |
| Vp | LS | e (h) | Vs | L4 | e (c) | AMPA | 3 | 9 | 0.8 | 7.5 |
| Vp | LS | e (h) | Vs | L4 | i (c) | AMPA | 3 | 9 | 0.8 | 7.5 |
| *Backward interareal connections* | | | | | | | | | | |
| Vs | LI | e (v) | Vp | LS | e (v) | NMDA | 25 | 25 | 0.1 | 7.5 |
| Vs | LI | e (v) | Vp | LS | i (v) | AMPA | 25 | 25 | 0.1 | 7.5 |
| Vs | LI | e (h) | Vp | LS | e (h) | NMDA | 25 | 25 | 0.1 | 7.5 |
| Vs | LI | e (h) | Vp | LS | i (h) | AMPA | 25 | 25 | 0.1 | 7.5 |
| Vs | LI | e (c) | Vp | LS | e (v) | NMDA | 25 | 25 | 0.1 | 7.5 |
| Vs | LI | e (c) | Vp | LS | i (v) | AMPA | 25 | 25 | 0.1 | 7.5 |
| Vs | LI | e (c) | Vp | LS | e (h) | NMDA | 25 | 25 | 0.1 | 7.5 |
| Vs | LI | e (c) | Vp | LS | i (h) | AMPA | 25 | 25 | 0.1 | 7.5 |
| **Thalamus** | | | | | | | | | | |
| *Thalamic connections* | | | | | | | | | | |
| Tp | | e | Rp | | i | AMPA | 5 | 5 | 1. 0 | 7.5 |
| Tp | | i | Tp | | e | GABA$_A$ | 5 | 5 | 0.3 | 7.5 |
| Tp | | i | Tp | | i | GABA$_A$ | 5 | 5 | 0.3 | 7.5 |
| Rp | | i | Tp | | e | GABA$_A$ | 25 | 25 | 0.1 | 7.5 |
| Rp | | i | Rp | | i | GABA$_A$ | 25 | 25 | 0.1 | 7.5 |
| Ts | | e | Rs | | i | AMPA | 5 | 5 | 1.0 | 7.5 |
| Ts | | i | Ts | | e | GABA$_A$ | 5 | 5 | 0.3 | 7. 5 |
| Ts | | i | Ts | | i | GABA$_A$ | 5 | 5 | 0.3 | 7. 5 |
| Rs | | i | Ts | | e | GABA$_A$ | 25 | 25 | 0.1 | 7.5 |
| Rs | | i | Rs | | i | GABA$_A$ | 25 | 25 | 0.1 | 7.5 |
| *Thalamocortical connections* | | | | | | | | | | |
| Tp | | e | Vp | L4 | e (v) | AMPA | 8 | 2 | 0.5 | 7.5 |
| Tp | | e | Vp | L4 | i (v) | AMPA | 8 | 2 | 0.5 | 7.5 |
| Tp | | e | Vp | LI | e (v) | AMPA | 8 | 2 | 0.3 | 7.5 |
| Tp | | e | Vp | LI | i (v) | AMPA | 8 | 2 | 0.3 | 7.5 |

**Table 3** – *continued*

| Source area | Layer | Cell type | Target area | Layer | Cell type | Synaptic channel | Arbor spread | | Max pr. of connection | Space constant |
|---|---|---|---|---|---|---|---|---|---|---|
| Tp |  | e | Vp | L4 | e (h) | AMPA | 2 | 8 | 0.5 | 7.5 |
| Tp |  | e | Vp | L4 | i (h) | AMPA | 2 | 8 | 0.5 | 7.5 |
| Tp |  | e | Vp | LI | e (h) | AMPA | 2 | 8 | 0.3 | 7.5 |
| Tp |  | e | Vp | LI | i (h) | AMPA | 2 | 8 | 0.3 | 7.5 |
| Ts |  | e | Vs | L4 | e (c) | AMPA | 4 | 4 | 0.5 | 7.5 |
| Ts |  | e | Vs | L4 | i (c) | AMPA | 4 | 4 | 0.5 | 7.5 |
| Ts |  | e | Vs | LI | e (c) | AMPA | 4 | 4 | 0.3 | 7.5 |
| Ts |  | e | Vs | LI | i (c) | AMPA | 4 | 4 | 0.3 | 7.5 |
| *Corticothalamic connections* | | | | | | | | | | |
| Vp | LI | e (v) | Tp |  | e | AMPA | 5 | 5 | 0.5 | 7.5 |
| Vp | LI | e (v) | Tp |  | i | AMPA | 5 | 5 | 0.5 | 7.5 |
| Vp | LI | e (v) | Rp |  | i | AMPA | 5 | 5 | 0.5 | 7.5 |
| Vs | LI | e (v) | Ts |  | e | AMPA | 5 | 5 | 0.4 | 7.5 |
| Vs | LI | e (v) | Ts |  | i | AMPA | 5 | 5 | 0.4 | 7.5 |
| Vs | LI | e (v) | Rs |  | i | AMPA | 5 | 5 | 0.4 | 7.5 |

(Kato, 1990). Other cortical areas which may serve as additional sources of common input to the modeled cortices were not included (Munk *et al.*, 1995). Such factors may account for the tight synchrony that was observed between the monkey V1 and V2 areas during gamma oscillations (Frien *et al.*, 1994). Indeed, the authors of this experimental study concluded that the near-zero synchronization was not due to reciprocal interactions between V1 and V2, but, rather, that it resulted from a source of common input to both areas.

In our model, changes in transmission latencies introduced to account for additional synaptic steps (see Materials and Methods) translated into distinct phase relationships between distributed neural activities (see Figs 2 and 8). These results raise the intriguing possibility that several coherent regimes with distinct phase relationships may occur within the same neural substrate as different sets of pathways come into play in a context-dependent manner. For example, the activation of centers with widespread projections (e.g. intralaminar thalamic nuclei and brainstem structures) may favor monosynaptic interactions that promote the onset of multi-level synchronous oscillations with near-zero phase lags. Such in-phase oscillations could correspond to the firing patterns observed during spontaneous activity (Steriade *et al.*, 1996a,b). On the other hand, the directed influences of external stimuli or of 'top-down' cortical processes may result in a stronger ordering of the activation along poly-synaptic loops and, therefore, in systematic phase-lags among distributed neural activities.

Synchronization within a single modeled cortical area occurred with small time lags (i.e. 0–4 ms). Other factors not included in the simulations could make this synchronization even tighter. Horizontal intralaminar connections were strictly confined to a single layer, while in reality these tangential connections can spread across layers to some degree. Moreover, we did not incorporate the synchronizing influence of the intralaminar thalamic nuclei, which have access to widespread cortical territories and straddle the cortical depth (Jones, 1985). These factors may be important in accounting for the extremely tight synchronization of fast cortical rhythms from surface to deep layers that has been recently recorded during spontaneous activity in the cat (Steriade *et al.*, 1996a).

### Concluding Remarks

We have developed the thalamocortical model described here as a base to explore some parameters and principles underlying the large-scale operations of the thalamocortical system and to test specific interpretations of neurophysiological data. The model has allowed us to investigate the specific role of several cortical and corticothalamic macro-circuits in generating and sustaining the fast, synchronous oscillatory activity that is observed in this system. In a companion paper, we will examine the effects of synchronous firing within these macro-circuits on neural processes subserving vision (Lumer *et al.*, 1997).

While the simulations presented in this paper do not yet address functional questions such as the genesis of orientation and directional selectivity (Wörgötter and Koch, 1991; Somers *et al.*, 1995; Douglas *et al.* 1995), the mechanisms of motion perception (Nowlan and Sejnowski, 1995), the neural basis of perceptual grouping and figure-ground segregation (Sporns *et al.*, 1991), the binding problem (Tononi *et al.*, 1992), or the mechanisms of visual attention (Lumer, 1992; Olshausen *et al.*, 1993; Niebur *et al.*, 1994), they provide a powerful tool to begin investigating these phenomena in closer contact with experimental observations.

### Appendix: Network Parameters

All connections activated their target channels with unitary strength, with the exception of thalamocortical projections which were four times stronger. Connectivity patterns are specified in Table 3 as follows: source area, layer of origin, and cell type (e, excitatory; i, inhibitory) and selectivity (v, vertical; h, horizontal; c, cross); target area, layer of termination, and cell type and selectivity; type of synaptic channel activated by the connection; size of the rectangular target area in which the projections from a single source cell diverge (expressed in number of topographic elements along vertical and horizontal axis in target map); maximum probability of connection at the center of the target area; space constant for the exponential fall-off of the probability of connection away from the center of the target area (expressed in number of topographic elements). Intrinsic cortical connections, corticothalamic projections from Vp to Tp and Rp, thalamocortical and corticothalamic projections from Vs to Ts and Rs, are isomorphic for the various selectivities; as a reference, we give in Table 3 the connectivity patterns originating from cells selective for vertical orientations. Thalamocortical projections from Tp to Vp and interareal projections are biased so as to produce feature selectivities;

these projections are described for all the selectivities present in the model.

## References

Ahmed B, Anderson J, Douglas R, Martin K, Nelson J (1994) Polyneuronal innervation of spiny stellate neurons in cat visual cortex. J Comp Neurol 341:39–49.

Baranyi A, Szente M, Woody C (1993) Electrophysiological characterization of different types of neurons recorded *in vivo* in motor cortex of the cat. II. membrane parameters action potentials. J Neurosci 69:1865–1879.

Beaulieu C, Colonnier M (1983) The numbers of neurons in different laminae of the binocular and monocular regions of area 17 in the cat. J Comp Neurol 217:337–344.

Beaulieu C, Colonnier M (1985) A laminar analysis of the number of round-asymmetrical and flat-symmetrical synapses on spines, dendritic trunks, and cell bodies in area 17 of the cat. J Comp Neurol 231:180–189.

Beaulieu C, Kisvárday Z, Somogyi P, Cynader M, Cowey A (1992) Quantitative distribution of GABA-immunonegative neurons and synapses in the monkey striate cortex (area 17). Cereb Cortex 2:295–309.

Bressler S (1995) Large-scale cortical networks and cognition. Brain Res Rev 20:288–304.

Bressler S, Coppola R, Nakamura R (1993) Episodic multiregional cortical coherence at multiple frequencies during visual task performance. Nature 366:153–156.

Bullier J, Henry C (1979) Neural path taken by afferent streams in striate cortex of the cat. J Neurophysiol 42:1264–1270.

Bullier J, McCourt M, Henry C (1988) Physiological studies on the feedback connection to the striate cortex from cortical area 18 and 19 of the cat. Exp Brain Res 70:90–98.

Bush P, Douglas R (1991) Synchronization of bursting action potential discharge in a model network of neocortical neurons. Neural Comp 3:19–30.

Callaway E, Wiser A (1994) Local circuits in macaque V1: projections of individual layer 2–5 neurons. Soc Neurosc Abstr 20:310.

Chagnac-Amital Y, Connors B (1989) Synchronized excitation and inhibition driven by intrinsically bursting neurons in neocortex. J Neurophysiol 62:1149–1162.

Cobb S, Buhl E, Halasy K, Paulsen O, Somogyi P (1995) Synchronization of neuronal activity in hippocampus by individual gabaergic interneurons. Nature 378:75–78.

Condé F, Lund J, Jacobowitz D, Baimbridge KU, Lewis D (1994) Local circuit neurons immunoreactive for calretinin, calbindin D-28k or parvalbumin in monkey prefrontal cortex: distribution and morphology. J Neurosci 341:95–116.

Connors B, Gutnick M (1990) Intrinsic firing patterns of diverse neocortical neurons. Trends Neurosci 13:99–104.

Connors B, Gutnick M, Prince D (1982) Electrophysiological properties of neocortical neurons *in vitro*. J Neurophysiol 48:1302–1320.

Damasio A (1989) The brain binds entities and events by multiregional activation from convergence zones. Neural Comp 1:123–132.

Destexhe A, Contreras D, Sejnowski T, Steriade M (1994) A model of spindle rhythmicity in the isolated thalamic reticular nucleus. J Neurophysiol 72:803–818.

Diamond I, Hall W (1969) The evolution of neocortex. Science 164:251–262.

Dinse H, Krüger K (1994) The timing of processing along the visual pathway in the cat. NeuroReport 5:893–897.

Douglas R, Martin K (1990) Neocortex. In: The synaptic organization of the brain (Shepherd G, ed). Oxford: Oxford University Press.

Douglas R, Koch C, Mahowald M, Martin K, Suarez H (1995) Recurrent excitation in neocortical circuits. Science 269:981–985.

Douglas R, Martin K, Witteridge D (1991) An intracellular analysis of the visual responses of neurones in cat visual cortex. J Physiol 1991:659–696.

Dubin M, Cleland B (1977) Organization of visual inputs to interneurons of lateral geniculate nucleus of the cat. J Neurophysiol 40:410–427.

Eckhorn R, Bauer R, Jordan W, Brosh M, Kruse W, Munk M, Reitboeck H (1988) Coherent oscillations: a mechanism of feature linking in the visual cortex? Multiple electrode and correlational analysis in the cat. Biol Cybernet 60:121–130.

Eggermont J (1990) The correlative brain. Berlin: Springer-Verlag.

Engel A, König P, Kreiter A, Singer W (1991a) Interhemispheric synchronization of oscillatory neuronal responses in cat visual cortex. Science 252:1177–1179.

Engel A, Kreiter A, König P, Singer W (1991b) Synchronization of oscillatory neuronal responses between striate ans extrastriate visual cortical areas of the cat. Proc Natl Acad Sci USA 88:6048–6052.

Felleman D, Van Essen D (1991) Distributed hierarchical processing in the primate cerebral cortex. Cereb Cortex 1:1–47.

Ferster D, Jagadeesh B (1992) Epsp–ipsp interactions in cat visual cortex studied with *in vivo* whole-cell patch recording. J Neurosci 12:1262–1274.

Fox K, Sato H, Daw N (1989) The location and function of NMDA receptors in cat and kitten visual cortex. J Neurosci 9:2443–2454.

Freund T, Martin K, Whitteridge D (1985) Innervation of cat visual areas 17 and 18 by physiologically identified X- and Y-type thalamic afferents. I. Arborization patterns and quantitative distribution of postsynaptic elements. J Comp Neurol 243:263–274.

Frien A, Eckhorn R, Bauer R, Woelbern T, Kehr H (1994) Stimulus-specific fast oscillations at zero phase between visual areas Vl and V2 of awake monkey. NeuroReport 5:2273–2277.

Gilbert C (1993) Circuitry, architecture, and functional dynamics of visual cortex. Cereb Cortex 3:373–386.

Girard P, Bullier J (1989) Visual activity in area V2 during reversible inactivation of area 17 in the macaque monkey. J Neurophysiol 62:1287–1302.

Girard P, Salin P, Bullier J (1991) Visual activity in macaque area V4 depends on area 17 input. NeuroReport 2:81–84.

Golomb D, Wang X.J, Rinzel J (1994) Synchronization properties of spindle oscillations in a thalamic reticular nucleus model. J Neurophysiol 72:1109–1126.

Gray C, Engel A, König P, Singer W (1992) Synchronization of oscillatory neuronal responses in cat striate cortex: temporal properties. Vis Neurosci 8:337–347.

Gray C, Singer W (1989) Stimulus-specific neuronal oscillations in orientation columns of cat visual cortex. Proc Natl Acad Sci USA 86:1698–1702.

Henry G, Salin P, Bullier J (1991) Projections from areas 19 and 18 to cat striate cortex: divergence and laminar specificity. Eur J Neurosci 3:186–200.

Hertz A, Creutzfeld O, Fuster J (1964) Statistiache eigenschaften der neuronaktivität in ascendierenden visuellen system. Kibernetik 2:61–71.

Hirsh J, Gilbert C (1991) Synaptic physiology of horizontal connections in the cat visual cortex. J Neurosci 11:1800–1809.

Jones E (1985) The thalamus. New York: Plenum Press.

Jones E (1993) Gabaergic neurons and their role in cortical plasticity in primates. Cereb Cortex 3:361–372.

Kang Y, Kaneko T, Ohishi H, Endo K, Araki T (1994) Spatiotemporally differential inhibition of pyramidal cells in the cat motor cortex. J Neurophysiol 71:280–293.

Kaplan E, Purpura K, Shapley R (1987) Contrast affects the transmission of visual information through the mammalian lateral geniculate nucleus. J Physiol 391:267–288.

Kato N (1990) Cortico-thalamo-cortical projection between visual cortices. Brain Res 509:150–152.

Kawaguchi Y (1995) Physiological subgroups of nonpyramidal cells with specific morphological characteristics in layer II/III of rat frontal cortex. J Neurosci 15:2638–2655.

Kim H, Connors B (1993) Apical dendrites of the neocortex: correlation between sodium- and calcium-dependent spiking and pyramidal cell morphology. J Neurosci 13:5301–5311.

Kisvárday Z, Eysel U (1992) Cellular organization of reciprocal patchy networks in layer III of cat visual cortex. Neuroscience 46:275 286.

Kisvárday Z, Eysel U (1993) Functional and structural topography of horizontal inhibitory connections in cat visual cortex. Eur J Neurosci 5:1558–1572.

Kisvárday Z, Kim DS, Eysel U, Bonhoeffer T (1994) Relationship between lateral inhibitory connections and the topography of the orientation map in cat visual cortex. Eur J Neurosci 6:1619–1632.

König P, Engel A, Löwel S, Singer W (1993) Squint affects synchronization of oscillatory responses in cat visual cortex. Eur J Neurosci 5:501–508.

Krubitzer L, Kaas J (1989) Cortical integration of parallel pathways in the visual system of primates. Brain Res 478:161–165.

Legéndy C, Salcman M (1985) Bursts and recurrences of bursts in the spike trains of spontaneously active striate cortex neurons. J Neurophysiol 53:926 939.

Le Vay S, Gilbert C (1976) Laminar patterns of geniculocortical projection in the cat. Brain Res 113:1–19.

Leventhal A (1979) Evidence that the different classes of relay cells of the cat's lateral geniculate nucleus terminate in different layers of the striate cortex. Exp Brain Res 37:349–372.

Lindström S, Wróbel A (1990) Frequency dependent corticofugal excitation of principal cells in the cat's dorsal lateral geniculate nucleus. Exp Brain Res 79:313–318.

Llinás R, Paré D (1991) Of dreaming and wakefulness. Neuroscience 44:521–535.

Llinás R, Ribary U (1993) Coherent 40-Hz oscillation characterizes dream state in humans. Proc Natl Acad Sci USA 90:2078–2081.

Llinás R, Grace A, Yarom Y (1991) In vitro neurons in mammalian cortical layer 4 exhibit intrinsic oscillatory activity in the 10- to 50-Hz frequency range. Proc Natl Acad Sci USA 88:897–901.

Löwel S, Freeman B, Singer W (1987) Topographic organization of the orientation column system in large flat-mounts of the cat visual cortex. J Comp Neurol 255:401–415.

Lumer E (1992) Selective attention to perceptual groups: the phase tracking mechanism. Int J Neural Systems 3:1–17.

Lumer E, Edelman G, Tononi G (1997) Neural dynamics in a model of the thalamocortical systen. II. the role of neural synchrony tested through perturbations of spike timing. Cereb Cortex 7:228–236.

MacGregor R (1987) Neural and brain modeling. New York: Academic Press.

Maex R, Orban G (1996) Model circuit of spiking neurons generating directional selectivity in simple cells. J Neurophysiol 75:1515–1545.

Mason A, Nicoll A, Stratford K (1991) Synaptic transmission between individual pyramidal neurons in the rat visual cortex in vitro. J Neurosci 11:72–84.

Maunsell J, Van Essen D (1983) The connections of the middle temporal visual area (MT) and their relationship to a cortical hierarchy in the macaque monkey. J Neurosci 3:2563–2586.

McCormick D, Gray C (1995) Physiologically identified cell groups have distinct receptive field and morphological properties in cat striate cortex. Soc Neurosc Abstr 21:1506.

Milner P (1974) A model for visual shape recognition. Psychol Rev 816:521.

Montero V (1991) A quantitative study of synaptic contacts on interneurons and relay cells of the cat lateral geniculate nucleus. Exp Brain Res 86:257–270.

Mountcastle V (1957) Modality and topographic properties of single neurons of cat's somatic sensory cortex. J Neurophysiol 20:408–434.

Munk M, Nowak L, Nelson J, Bullier J (1995) Structural basis of cortical synchronization. II. Effects of cortical lesions. J Neurophysiol 74.

Murthy V, Fetz E (1992) Coherent 25- to 35-Hz oscillations in the sensorimotor cortex of awake behaving monkeys. Proc Natl Acad Sci USA 89:5670–5674.

Nelson J, Salin P, Munk NI, Arzi NI, Bullier J (1992) Spatial and temporal coherence in corticocortical connections: a cross-correlation study in areas 17 and 18 in the cat. Vis Neurosci 9:21–27.

Neuenschwander S, Singer W (1996) Long-range synchronization of oscillatory light responses in the cat retina and lateral geniculate nucleus. Nature 379:728–733.

Nicolelis M, Baccala L, Lin R, Chapin J (1995) Sensorimotor encoding by synchronous neural ensemble activity at multiple levels of the somatosensory system. Science 268:1353–1358.

Niebur E, Koch C (1994) A model for the neuronal implementation of selective visual attention based on temporal correlation among neurons. J Comput Neurosci 1:141–158.

Nowlan S, Sejnowski T (1995) A selection model for motion processing in area MT of primates. J Neurosci 15:1195–1214.

Olshausen B, Anderson C, Van Essen D (1993) A neural model of visual attention and invariant pattern recognition based on dynamic routing of information flow. J Neurosci 13:4700–4719.

Oram M, Perett D (1992) Time course of neural responses discriminating different views of the face and head. J Neurophysiol 68:70–84.

Otis T, Koninck YD, Mody I (1993) Characterization of synaptically elicited GABA_B responses using patch-clamp recordings in rat hippocampal slices. J Physiol 463:391–407.

Otis T, Mody I (1992) Differential activation of GABA_A and GABA_B receptors by spontaneously released transmitter. J Neurophysiol 67:227–235.

Payne B (1993) Evidence for visual cortical area homologs in cat and macaque monkey. Cereb Cortex 3:1–25.

Peters A, Payne B (1993) Numerical relationships between geniculo-cortical afferents and pyramidal cell modules in cat primary visual cortex. Cereb Cortex 3:69–78.

Peters A, Yilmaz E (1993) Neuronal organization in area 17 of cat visual cortex. Cereb Cortex 3:49–68.

Pinault D, Deschênes N (1992) Voltage-dependent 40-Hz oscillations in rat reticular thalamic neurons in vivo. Neuroscience 51:245–258.

Press W, Teukolsky S, Vettering W, Flannery B (1992) Numerical recipes in C, 2nd edn. Cambridge: Cambridge University Press.

Rakic P (1995) A small step for the cell, a giant step for mankind: a hypothesis of neocortical expansion during evolution. Trends Neurosci 18:383–388.

Robson J (1983) The morphology of corticofugal axons to the dorsal lateral geniculate nucleus in the cat. J Comp Neurol 216:89–103.

Rockland K (1992) Configuration, in serial reconstruction, of individual axons projecting from area V2 to V4 in the macaque monkey. Cereb Cortex 2:353–374.

Rockland K, Pandya D (1979) Laminar origins and terminations of cortical connections of the occipital lobe in the rhesus monkey. Brain Res 179:3–20.

Rockland K, Saleem K, Tanaka K (1994) Divergent feedback connections frorn areas V4 and TEO in the macaque. Vis Neurosci 11:579–600.

Rockland K, Virga A (1989) Terminal arbors of individual 'feedback' axons projecting from area V2 to V1 in the macaque monkey: a study using immunohistochemistry of anterogradely transported phaseolus vulgaris-leucoagglutinin. J Comp Neurol 285:54–72.

Rockland KS, Hoesen UV (1994) Direct temporal-occipital feedback connections to striate cortex (V1) in the macaque monkey. Cereb Cortex 4:300–313.

Rosenquist A (1985) Connections of visual cortical areas in the cat. In: Cerebral Cortex (Peters A, Jones E, eds), vol. 2, chap. 3, pp. 81–117. New York: Plenum.

Rosier A, Arckens L, Orban G, Vandesande F (1993) Laminar distribution of NMDA receptors in cat and monkey visual cortex visualized by [$^3$H]-MK-801 binding. J Comp Neurol 335:369–380.

Salin PA, Bullier J (1995) Corticocortical connections in the visual system: structure and function. Physiol Rev 75:107–154.

Sanseverino E, Agnati L, Maioli M, Galletti C (1973) Maintained activity of single neurons in striate and non-striate areas of the cat visual cortex. Brain Res 54:225–242.

Schuster H (1988) Deterministic chaos. Weinheim: VCH Verlag.

Shipp S, Zeki S (1989) The organization of connections between areas V5 and V2 in macaque monkey visual cortex. Eur J Neurophysiol 1:333–354.

Sillito A, Jones H, Gerstein G, West D (1994) Feature-linked synchro-nization of thalamic relay cell firing induced by feedback from the visual cortex. Nature 369:479–482.

Singer W (1993) Synchronization of cortical activity and its putative role in information processing and learning. Annu Rev Physiol 55:349–374.

Somers D, Nelson S, Sur M (1995) An emergent model of orientation selectivity in cat visual cortical simple cells. J Neurosci 15:5448–5465.

Somogyi P, Cowey A (1984) Double bouquet cells. In: Cerebral Cortex (Peters A, Jones E, eds), vol. 1, chap. 9, pp. 337–360. New York: Plenum.

Sporns 0, Tononi G, Edelman G (1991) Modeling perceptual grouping and figure-ground segregation by means of active reentrant connections. Proc Natl Acad Sci USA 88:129–133.

Stemmler M, Usher D, Niebur E (1995) Lateral interactions in primary visual cortex: a model bridging physiology and psychophysics. Science 269:1877–1880.

Steriade M, Amzica F, Contreras D (1996a) Synchronization of fast (30–40

Hz) spontaneous cortical rhythms during brain activation. J Neurosci 16:392–417.

Steriade M, Contreras D, Amzica F, Timofeev I (1996b) Synchronization of fast (30–40 Hz) spontaneous oscillations in intrathalamic and thalamocortical networks. J Neurosci 16:2788–2808.

Steriade M, Dossi RC, Contreras D (1993) Electrophysiological properties of intralaminar thalamocortical cells discharging rhythmic (~40 hz) spike-bursts at ~1000 Hz during waking and rapid eye movement sleep. Neuroscience 56:1–9.

Steriade M, Dossi RC, Paré D, Oaks U (1991) Fast oscillations (20–40 hz) in thalamocortical systems and their potentiation by mesopontine cholinergic nuclei in the cat. Proc Natl Acad Sci USA 88:4396–4400.

Stern P, Edwards F, Sakmann B (1992) Fast and slow components of unitary EPSCs on stellate cells elicited by focal stimulation in slices of rat visual cortex. J Physiol 449:247–278.

Swadlow H (1988) Efferent neurons and suspected interneurons in binocular visual cortex of the awake rabbit: receptive fields and binocular properties. J Neurophysiol 59:1162–1187.

Tononi G, Sporns O, Edelman G (1992) Reentry and the problem of integrating multiple cortical areas: simulation of dynamic integration in the visual system. Cereb Cortex 2:310–335.

Traub R, Miles R, Wong R (1989) Model of the origin of rhythmic population oscillations in hippocampal slice. Science 243:1319–1325.

von der Malsburg C (1981) The correlation theory of the brain. Internal report, Max Planck Institute for Biophysical Chemistry, Gottingen.

Weber A, Kalil R, Behan M (1989) Synaptic connections between corticogeniculate axons and interneurons in the dorsal lateral geniculate nucleus of the cat. J Comp Neurol 289:156–164.

Whittington M, Traub R., Jefferys J (1995) Synchronized oscillations in interneuron networks driven by metabotropic glutamate receptor activation. Nature 373:612–615.

Wilson M, Bower J (1989) The simulation of large-scale neural networks. In: Methods in neuronal modeling (Koch C, Segev I, eds), chap. 9, pp. 291–333. Cambridge, MA: MIT Press.

Wilson M, Bower J (1992) Cortical oscillations and temporal interactions in a computer simulation of piriform cortex. J Neurophysiol 67:981–995.

Wiser A, Callaway E (1994) Local circuits in macaque V1: projections of individual layer 6 neurons. Soc Neurosci Abstr 20:310.

Wörgötter F, Koch C (1991) A detailed model of the primary visual pathway in the cat: comparison of afferent excitatory and intracortical inhibitory connection schemes for orientation selectivity. J Neurosci 11:1959–1979.

Zeki S, Shipp S (1988) The functional logic of cortical connections. Nature 335:311–317.

Zeki S, Shipp S (1989) Modular connections between areas V2 and V4 of macaque monkey visual cortex. Eur J Neurosci 1:494–506.